WestVirginiaUniversity
THE RESEARCH REPOSITORY @ WVU

Graduate Theses, Dissertations, and Problem Reports

2016

Application of computer vision for roller operation management

Mohammad Hadi Niki Rashidi

Follow this and additional works at: https://researchrepository.wvu.edu/etd

Recommended Citation

Niki Rashidi, Mohammad Hadi, "Application of computer vision for roller operation management" (2016). *Graduate Theses, Dissertations, and Problem Reports*. 7337.
https://researchrepository.wvu.edu/etd/7337

This Dissertation is protected by copyright and/or related rights. It has been brought to you by the The Research Repository @ WVU with permission from the rights-holder(s). You are free to use this Dissertation in any way that is permitted by the copyright and related rights legislation that applies to your use. For other uses you must obtain permission from the rights-holder(s) directly, unless additional rights are indicated by a Creative Commons license in the record and/ or on the work itself. This Dissertation has been accepted for inclusion in WVU Graduate Theses, Dissertations, and Problem Reports collection by an authorized administrator of The Research Repository @ WVU. For more information, please contact researchrepository@mail.wvu.edu.

APPLICATION OF COMPUTER VISION FOR ROLLER OPERATION MANAGEMENT

Mohammad Hadi Niki Rashidi

Dissertation submitted
to the Statler College of Engineering and Mineral Resources
at West Virginia University

in partial fulfillment of the requirements for the degree of
Doctor of Philosophy in
Civil Engineering

John P. Zaniewski, Ph.D., Chair
Yoojung Yoon, Ph.D.
Avinash Unnikrishnan, Ph.D.
Fei Dai, Ph.D.
Yaser Fallah, Ph.D.

Department of Civil and Environmental Engineering

Morgantown, West Virginia

2016

Keywords: Construction, Intelligent Compaction, Computer Vision, Infrared

Copyright 2016 Mohammad Hadi Niki Rashidi

ProQuest Number: 10115792

All rights reserved

INFORMATION TO ALL USERS
The quality of this reproduction is dependent upon the quality of the copy submitted.

In the unlikely event that the author did not send a complete manuscript
and there are missing pages, these will be noted. Also, if material had to be removed,
a note will indicate the deletion.

ProQuest 10115792

Published by ProQuest LLC (2016). Copyright of the Dissertation is held by the Author.

All rights reserved.
This work is protected against unauthorized copying under Title 17, United States Code
Microform Edition © ProQuest LLC.

ProQuest LLC.
789 East Eisenhower Parkway
P.O. Box 1346
Ann Arbor, MI 48106 - 1346

ABSTRACT

APPLICATION OF COMPUTER VISION FOR ROLLER OPERATION MANAGEMENT

Mohammad Hadi Niki Rashidi

Compaction is the last and possibly the most important phase in construction of asphalt concrete (AC) pavements. Compaction densifies the loose (AC) mat, producing a stable surface with low permeability. The process strongly affects the AC performance properties. Too much compaction may cause aggregate degradation and low air void content facilitating bleeding and rutting. On the other hand too little compaction may result in higher air void content facilitating oxidation and water permeability issues, rutting due to further densification by traffic and reduced fatigue life. Therefore, compaction is a critical issue in AC pavement construction.

The common practice for compacting a mat is to establish a roller pattern that determines the number of passes and coverages needed to achieve the desired density. Once the pattern is established, the roller's operator must maintain the roller pattern uniformly over the entire mat.

Despite the importance of uniform compaction to achieve the expected durability and performance of AC pavements, having the roller operator as the only mean to manage the operation can involve human errors.

With the advancement of technology in recent years, the concept of intelligent compaction (IC) was developed to assist the roller operators and improve the construction quality. Commercial IC packages for construction rollers are available from different manufacturers. They can provide precise mapping of a roller's location and provide the roller operator with feedback during the compaction process.

Although, the IC packages are able to track the roller passes with impressive results, there are also major hindrances. The high cost of acquisition and potential negative impact on productivity has inhibited implementation of IC.

This study applied computer vision technology to build a versatile and affordable system to count and map roller passes. An infrared camera is mounted on top of the roller to capture the operator view. Then, in a near real-time process, image features were extracted and tracked to estimate the incremental rotation and translation of the roller. Image featured are categorized into near and distant features based on the user defined horizon. The optical flow is estimated for near features located in the region below the horizon. The change in roller's heading is constantly estimated from the distant features located in the sky region. Using the roller's rotation angle, the incremental translation between two frames will be calculated from the optical flow. The roller's incremental rotation and translation will put together to develop a tracking map.

During system development, it was noted that in environments with thermal uniformity, the background of the IR images exhibit less featured as compared to images captured with optical cameras which are insensitive to temperature. This issue is more significant overnight, since nature elements are not able to reflect the heat energy from sun. Therefore to improve roller's heading estimation where less features are available in the sky region a unique methodology that

allows heading detection based on the asphalt mat edges was developed for this research. The heading measurements based on the slope of the asphalt hot edges will be added to the pool of the headings measured from sky region. The median of all heading measurements will be used as the incremental roller's rotation for the tracking analysis.

The record of tracking data is used for QC/QA purposes and verifying the proper implementation of the roller pattern throughout a job constructed under the roller pass specifications.

The system developed during this research was successful in mapping roller location for few projects tested. However the system should be independently validated.

DEDICATION:

To my parents, Mehri and Hamid, and to my brothers, Mehdi and Javad, without whom none of my success would have been possible.

ACKNOWLEDGMENT

I would like to give special thanks to Dr. John Zaniewski my advisor, who has given me a vast degree of encouragement and support throughout this study. I also would like to express my deep appreciation to my committee members Dr. Avinash Unnikrishnan, Dr. Fei Dai, Dr. Yoojung Yoon, and Dr. Yaser P. Fallah for their valuable time, helpful suggestions, and great support on my research.

I appreciate all the support and help from research engineers at West Virginia Department of Transportation, Mr. Donald Williams and Michael Pumphrey. In addition, I would like to thank my late friend and the former West Virginia State Pavement Engineer, Mr. Thomas Medvick.

I want to express my sincerest appreciation and love to my family for providing me with endless support and opportunities throughout my life.

Last but not least, my best friends, Mehrdad Shahabi, Mehrdad Mohtadi, Ali Abutalebpur, Amirhossein Houshmandyar, Mehdi Shahbazi, and Justin Pintz in Morgantown, with whom I had the most memorable moments during my studies.

TABLE OF CONTENT

LIST OF FIGURES

LIST OF TABLES

NOMENCLATURE/LIST OF ACRONYMS

Chapter 1: **INTRODUCTION**

1.1. COMPACTION SIGNIFICANCE

Asphalt concrete (AC) is a mixture of aggregate and asphalt binder. The AC is the major material used in paving surface of roads, airfields and parking lots. AC pavements are required to be stable under the traffic loads, smooth, durable and impermeable unless designed otherwise. To achieve the expected properties and performance, the loose AC mixture placed by a paver must be compacted during the construction.

Compaction is the process of reducing the volume of loose AC material under an external force applied by rollers. The compaction force squeezes loose asphalt-coated aggregates together providing increased aggregate interlock and stronger asphalt bonds for higher stability to endure traffic loads.

In order to achieve the specified density uniformly all over the surface, a plan for compaction is required. This plan is called rolling pattern and should define the quantity of rollers, roller types, rolling sequences, speed, length of rolling zone and number of passes made by each roller. A “pass” is referred to the roller passing over a surface **point** once. The total passes required to cover the whole width of mat being paved is one “coverage”. Figure 1, illustrate a rolling pattern comprised of 8 passes and 2 coverages.

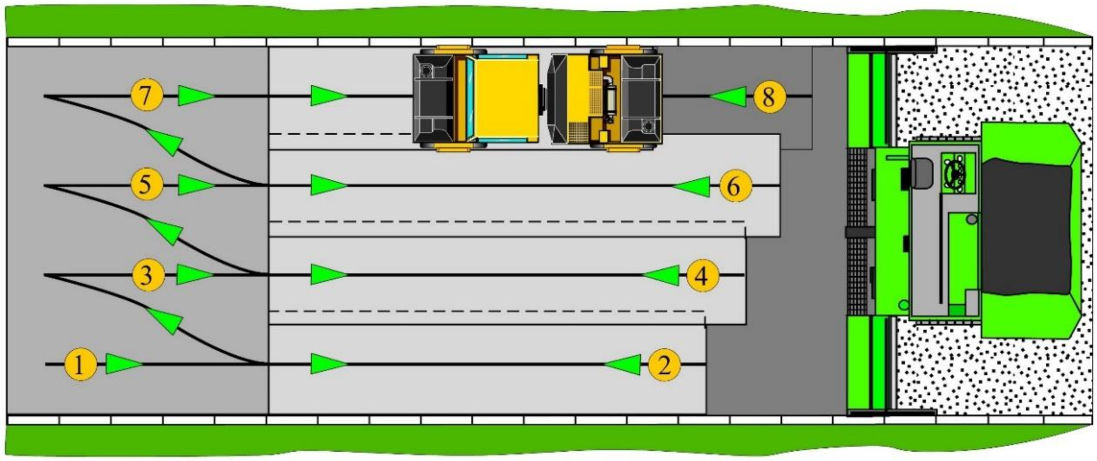

Figure 1 Roller Pass and Coverage (Source: BOMAG)

1.2. INTELLIGENT COMPACTION

The roller operator is in charge for maintaining the rolling pattern as consistent as possible. Remembering the rolling zone limits and keeping track of number of passes and coverages is tedious, but it is essential to achieve the target density and compaction uniformity. To assist roller operators and minimizing human errors intelligent compaction (IC) was developed.

Currently commercial IC packages are available in the market from several manufacturers. Figure 2 describes the most comprehensive available package. This IC system is comprised of data acquisition sensors, automatic feedback control (AFC) and output devices such as a display screen and a printer. The data acquisition part includes an accelerometer for drum vibration measurement, infrared temperature detectors, and GPS. The AFC unit analyzes the acquired data and adjusts vibration accordingly. The operator screen also displays helpful information such as the mat temperature, estimated mat density, vibration frequency and amplitude, vibration mode, pass mapping and density map.

Not all the IC packages cover all the activities in Figure 2. The AFC unit can only be used on rollers with directional compaction technology, which are not very common. IC packages mostly focus on pass mapping, temperature records, and possibly density map for vibratory rollers.

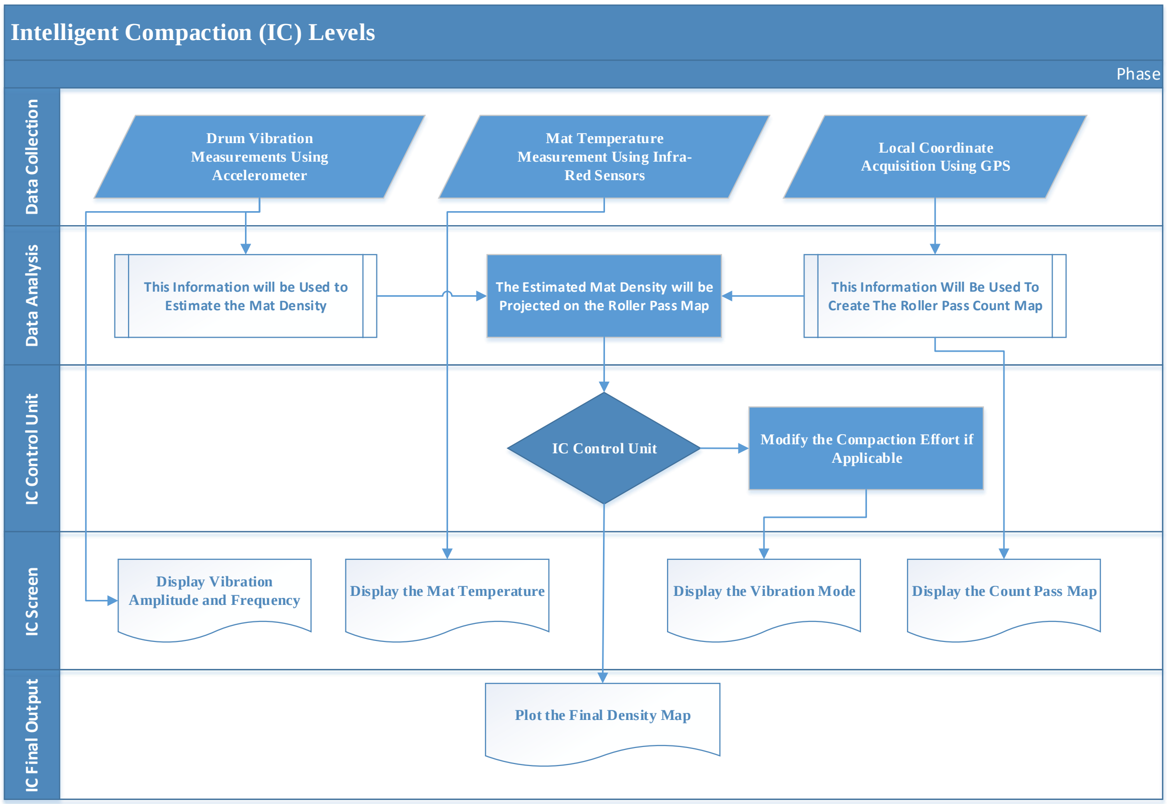

Figure 2 Comprehensive IC Flowchart

The current IC packages available use global positioning system (GPS) to map the roller location. Despite the satisfactory results, these systems have two disadvantages that make contractors reluctant to adopt this technology. First, because the functionality of these packages highly depends on the precision of the real time location information, a sophisticated GPS antenna is required. This increases the price of typical new vibratory tandem asphalt roller by almost 20%-25% (based on the quotation for Trimble CSS Flex, dated August 2012). For most of the contractors who already own a compaction fleet, the investment may be greater than the current value of their equipment.

Moreover, the GPS device integrated into the IC require stationary support. Single or multiple reference stations on the job site are needed to constantly correct the satellite data acquired by the GPS mounted on the roller. To maintain the system functionality, it is essential to keep the radio line of sight between the antenna mounted on the roller and stationary GPS antennas clear. As the paving train moves forward the line of sight may be lost, especially in the terrain of West Virginia. When the line of sight is interrupted, the stationary antennas must be reset and the paving process is either stopped or operates without IC.

1.3. PROBLEM STATEMENT

Currently the industry is seeking a solution to improve AC construction quality and reduced labor effort for QC/QA through intelligent monitoring of AC compaction. As discussed earlier, the shortcomings of the existing solutions has kept the IC away from being widely accepted and becoming a standard practice.

1.4. OBJECTIVE

The objective of this research was to design and build an economical IC package that can be used on any asphalt compaction roller to produce roller pass mapping for assisting the operator during the operation and collect data that can be used for QC/QA.

1.5. SCOPE AND LIMITATIONS

The proposed configuration consisted of a long wave infrared (LWIR) camera, a triple suction cup camera mount, a 7in display screen and a data logger integrated with an accelerometer and a

GPS. LWIR Camera, is implemented to capture the operator's vision. The LWIR technology detects the thermal radiation emitted from the surface, hence, it improves image processing efforts for distinguishing the hot mat from the surrounds.

To address the objective of making the system as economical as practical, trade-offs were made between the capability of the equipment and costs. The biggest trade-off was on the selection of the LWIR camera. Although more information could be captured with a color camera, a black and white camera was selected for the sake of economy.

Different optical cameras were also tested in this study. This was done to verify if a sole optical camera could be used for roller tracking. The comparison of performance and applications was used to justify the need for an IR camera.

OpenCV library was used to do real-time image processing inside C++ and C#. Finally, the processed information regarding the rolling operation including the pass map was plotted on the display screen.

The goal of any compaction operation is to build a finished surface to the required density, uniformly. To achieve this goal various parameters including mixture properties (gradation, asphalt binder content, mix type, mix temperature), environmental effects, layer thickness, available time, subgrade or base condition and compaction energy are involved. With regard to parameters involved in a successful compaction operation this study only addresses the roller operation.

The result of this research is only applicable to hot mix asphalt (HMA) and warm mix asphalt (WMA) paving. Compaction of granular courses and cold mix asphalt (CMA) are not part of the scope of this research.

Depending on the size of the construction project, time available for compaction and rollers availability, a single or a group of rollers maybe used to perform the compaction. The current research is limited to the single roller operation. On projects where more than one roller is involved in a rolling zone, it is possible to use the product of this research on each roller individually. A multi-user version of the device is desirable but beyond the scope of this project.

AC pavement constructions are performed both during the day and night. In fact, many of overlay projects are placed during the night to minimize traffic disturbance. Using the LWIR technology, the result of this research delivers satisfactory results both on day and night jobs.

1.6. JUSTIFICATION

In this study, GPS technology of commercial IC is replaced by computer vision technology to build an IC package for roller pass mapping. The new device offers a considerably lower price compared to the current commercial IC packages available in the market which promotes its practicality. In addition, the device performs as an independent unit without requiring any stationary/remote support which eliminates part of the current IC limitations.

Chapter 2: **LITERATURE REVIEW**

2.1. INTRODUCTION

Due to the wide variety of the topics discussed in this chapter, the materials are organized in three sections. Section 2.2 briefly discusses major parameters affecting asphalt concrete (AC) compaction. Section 2.3 introduces the intelligent compaction and its state of practice. Section 2.4 covers the computer vision application and focuses on methods of perceiving the environment, image processing and simultaneous localization and mapping.

2.2. ASPHALT CONCRETE COMPACTION

Compaction is the process through which a mass of material loses volume or in other words densifies. For AC, compaction locks the aggregate particles together, providing stability, resistance to deformation and improved longevity by reducing permeability. To achieve the target density at field, it is essential to study the affecting factors. These factors can be categorized in mixture properties, environmental conditions, lift thickness and the condition of underlying structure [1].

2.2.1. Mixture Properties

Mixture properties such as aggregate size and gradation, binder content and type, mix design and mat temperature can greatly affect the mixture workability and resistance to the roller compaction. Therefore, a successful compaction starts with the proper choice of ingredients, mixture preparation and handling [1].

Mixture workability and compactibility

Cabrera [2] refer to workability as “the property which allows the production, handling, placing and compaction of a mix with minimum application of energy”. Compactibility is a component of workability which determines the ability of a material to be compressed into a compact mass. The workability is influenced by aggregate type, shape and gradation, asphalt binder percentage and grade, and mix temperature.

Aggregate

Angularity, shape, surface texture, gradation and filler properties can alter the mixture workability. Usually coarse mixtures tend to have less workability and requires more compaction effort for packing [1].

Mix Design

Mix designs normally fall in either dense graded, gap graded or stone mastic asphalt (SMA) categories. Each of these mix types behave differently in respond to compaction. Mix design is performed to find the right gradation and percent binder for the mixture of interest. Gradation defines the configuration of aggregate structure in the mix and can highly affect the mixture compactibility. Binder serves as lubricant helping aggregate displacement during compaction and generally mixtures with higher binder content are easier to compact [1].

2.2.2. Temperature

Asphalt Binder

Asphalt binder is a viscoelastic material, consequently, its behavior changes with the temperature. Asphalt binder viscosity decreases with temperature increase. McLeod [3] showed a 10,000-fold increase asphalt viscosity with temperature drop from 135 ºC to 57 ºC (275º-135ºF). This shows temperature can be used to adjust the mixture workability. The rate of asphalt reaction to the temperature change depends on the binder grade. At 121º-149 ºC (250º-300ºF) asphalt behaves as a liquid and the viscosity is sufficiently low for coating aggregate and mixture production. Construction at this temperature range allows aggregate pass each other under the roller drum easily, without any resistance from the asphalt binder; it actually serves as lubricant. As the mat temperature drops, the asphalt binder viscosity increase and provides resistance to the compaction. Mixture resistance to compaction increases to almost 10-fold as temperature drops from 135 ºC to 63 ºC (275º-145ºF) [3]. In practice for HMA at temperatures below 80 ºC (175ºF) very little, if any, increase in density can be achieved by rolling [1].

Mix Temperature

For HMA, the mixture production temperature must be enough to enable asphalt binder coat aggregate particles thoroughly and uniformly. Higher production temperature also provides longer time period for effective rolling and compaction at the field. Generally, the asphalt temperature should not exceed 170 ºC (338ºF) during the production process [1].

Mix temperature at the time of compaction is a function of production temperature, thermal properties of the mix, paving process, HMA mat thickness and environmental conditions including air temperature, base temperature, wind velocity and solar flux [4].

Monitoring mat temperature is particularly crucial in cold weather. McLeod [3] showed excessive premature distresses in such conditions. He also demonstrated that mixtures compacted to 95 percent of their laboratory compacted density showed 77 percent lower Marshall stability compared to those compacted to 100 percent. Cabrera [2] also detected reduced tensile strength and resilient moduli of asphalt concrete for mixes compacted at lower temperatures.

Due to the significant effect of temperature on compaction of HMA, it is important to plan the compaction strategy based on the time availability. This requires an understanding of heat transfer in the HMA mat during the paving operation in order to develop a model that can predict the time available for compaction. Chadboum et al [4], developed the “PaveCool” software for the Minnesota Department of Transportation. PaveCool predicts the HMA mat cooling rate based on a model and numerical solution presented by Luoma, et al [5].

With WMA, production normally takes place at temperatures 15 ºC to 35 ºC (30 °F to 70 °F) lower than HMA and remain lower during hauling, placement and compaction. Due to the use of chemical additives or foaming technology which allow mixing asphalt binder with aggregates at lower temperature, it is easier to manipulate and compact the WMA at lower temperatures [6].

2.2.3. Environmental Effects

Environmental condition of the construction site can affect the time available for compaction. Time available for compaction is the period of time that compaction can be achieved before the temperature drops below80 ºC 175ºF, for HMA [1].

Environmental condition includes the air and underlying surface temperatures, wind speed and solar flux. Solar flux is the amount of radiant energy received from the sun and is a factor of various variables such as altitude, cloud density, haze level and position of the sun relative to the horizon which itself is a variable of the time of the day and year [7].

2.2.4. Lift Thickness

Compaction of thicker HMA lifts is easier in general. Thicker asphalt mats tend to preserve the mat temperature for a longer period of time providing longer time for compaction [1].

2.2.5. Underlying Structure Condition

Underlying surface condition can affect the compaction results in different ways. Wet or cool surfaces absorb the heat from the AC lift being paved and reduce the time available for compaction. Uneven surfaces lead to non-uniform lift thicknesses and non-uniform compaction results consequently. Instability in the underlying structure can result in lack of bottom confinement required to achieve the density [1].

2.2.6. Rolling operation

In general, using rollers to compact the AC layer on the field takes place in 3 steps “break - down”, “intermediate” and “finish”. The break-down roller gets the initial and the majority of the density, the target density is supposed to be achieved with the intermediate rolling and finally the finish roller removes the marks and surface defects. Single or multiple rollers can be assigned to the tasks depending on the time available for compaction and the paving rate [7].

The rolling pattern is unique for each project, since the mixture type and properties, lift thickness, environment, underlying surface density and rollers availability vary. To establish a rolling pattern, a test strip needs to be built at the beginning of each project to simulate the rolling operation using the actual material, thickness, environmental and underlying surface conditions. Then the non-destructive density gauges are used to measure the in-place density after each pass. The data collected helps to find the optimum number of passes for each participating roller to establish the rolling pattern and approximate rolling zone [1].

2.2.7. Roller Types

To perform the compaction task in the field several different roller types have been developed to raise the process efficiency. Generally, the asphalt compaction rollers are categorized as:

- Tandem steel rollers, static and dynamic
- Pneumatic rollers
- Combination of steel drum and tires

Furthermore, construction rollers can be classified into static and vibratory rollers, based on the state of energy applied to the surface.

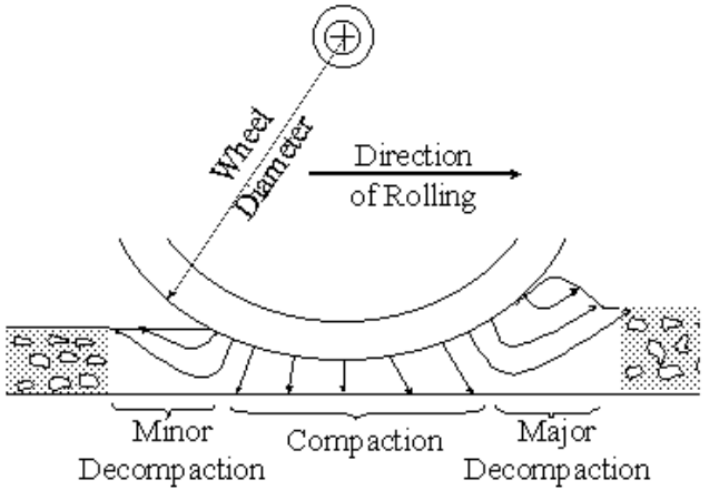

Figure 3 Drum Action [8].

Static Tandem Roller

The static tandem steel rollers use their gross weight and possibly add-on loads to press down the mat in order to get the density. The term static indicates the compaction force is due to the static weight of roller. As shown in Figure 4-(a) the exerted compaction force for this type of rollers is expressed in terms of static linear load, which is a factor of roller gross weight, and the width and diameter of the drums. The drum contact area is a narrow band which contracts in length as the loose mat become densified with the subsequent roller passes, see Figure 4-(b) for illustration. As the contact area reduces, the contact pressure on the surface increases [7].

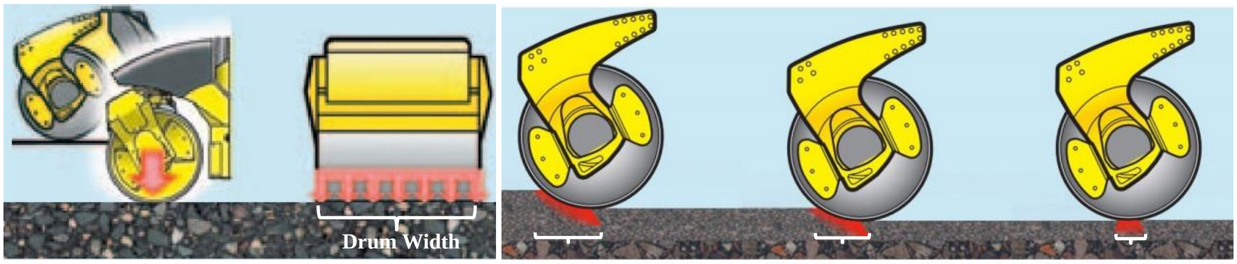

(a) Linear Load (b) Drum Contact Length

Figure 4 Static Tandem Roller [9]

Dynamic rollers

Traditional dynamic rollers have either one or two drums with a system of eccentric weights spinning around the center shaft. The centrifugal force created by the spinning eccentric weight(s) causes vertical displacement of the drum. In fact, drum in vibratory mode not only rolls over the mat but it also beats the surface. Dynamic compaction can greatly improve the compaction results. The vibration helps the aggregate to relocate and reorient in the mat, allowing achievement of a denser configuration. Moreover, because of the impact action due to drum vertical displacement the compaction force increases considerably.

Figure 5-(a) shows the mechanism used in traditional dynamic rollers. These type rollers normally come with a single circular exciter at the center of the drum. Spinning the exciter at high speed induces vibration in the drum. The vibration frequency or in other words the number of drum’s impacts within a unit time period, can be controlled by changing the exciter spinning speed. Counter weights shown in Figure 5-(b) might be used to adjust the magnitude of the impacts.

(a) The Exciter Full Cycle (b) The Counter Weight Action

Figure 5 Traditional Vibratory Rollers [10]

The later generation of vibratory rollers takes the advantage of a new vibration mechanism often known as directed vibration. Figure 6, displays the directed vibration mechanism. Such systems use two counter-rotating eccentric weights. The magnitude of the centrifugal force reaches its maximum peak when the two weights spin in the same direction. They can also partially balance each other out, if rotated in opposite direction. Directional systems are also capable of adjusting the vibration magnitude, by changing the orientation of the whole vibration system. As the system orientation deviates from the vertical axis, the produced centrifugal force disintegrates into horizontal and vertical vectors reducing the magnitude of the vertical impact. The horizontal vibration improves the surface finish [9].

Despite all the benefits associated with vibration, it comes with two problems. First, the drum loses contact with the surface between consecutive impacts. Second, the surface marks created by drum impacts, especially when operated in high amplitude mode. To solve these issues oscillatory rollers were introduced.

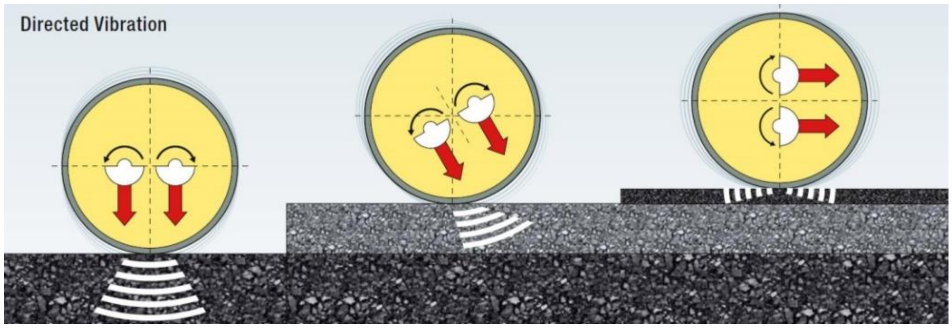

Figure 6 Directed Vibration [9]

Figure 7, compare oscillation and vibration mechanisms. Oscillation only induces horizontal displacements, thus, it maintains the drum in permanent contact with the surface. Compared to the vibratory rollers, oscillatory rollers can greatly improve the surface finish but their compaction influence depth is shallower [9].

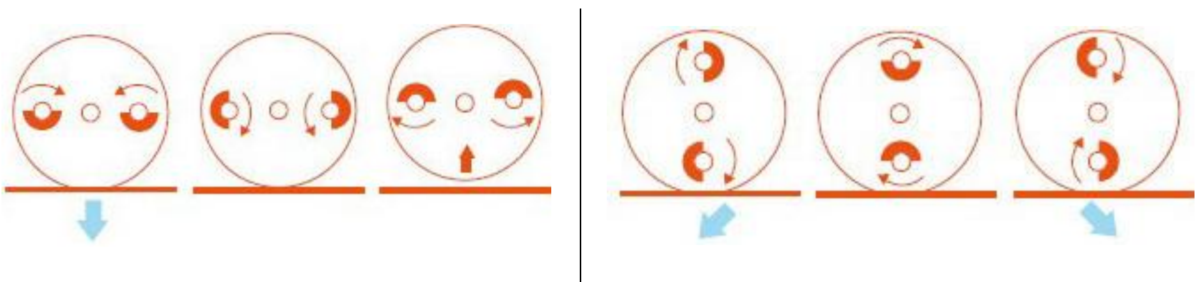

(a) Vibration Mechanism (b) Oscillation Mechanism

Figure 7 Comparison of Vibration and Oscillation [10]

All dynamic steel wheel rollers can also be operated in static mode, therefore they can be used for all phases of compaction process.

Pneumatic Tire Roller

The pneumatic rollers, in Figure 8-(a), generally serve as the intermediate roller operating behind the break down roller. The rear tires are shifted to cover the areas not compacted by the front wheels, see Figure 8-(b) for illustration.

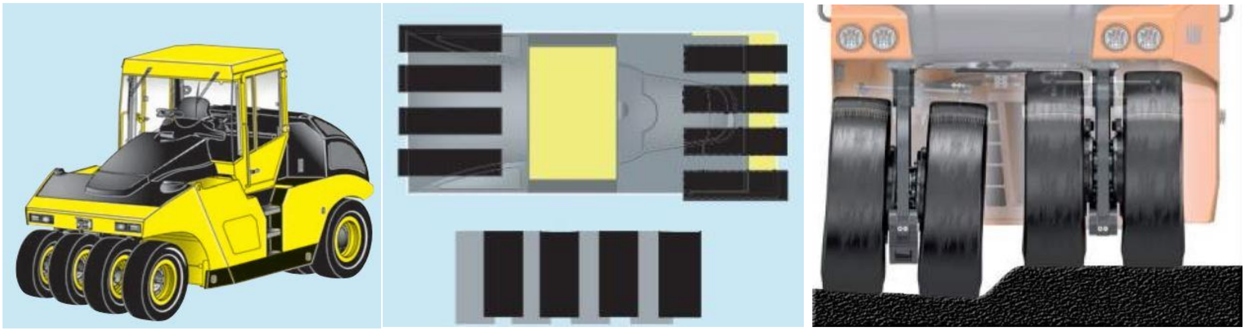

(a) Pneumatic Roller (b) Tires Formation (c) Tires on Uneven Surfaces

Figure 8 Pneumatic Tire Roller Illustration [9]

The compaction force of the pneumatic rollers is applied by tires. The compaction energy is a factor of roller gross weight, tire pressure and tire design. As displayed in Figure 8-(c), unlike the steel drum rollers where the solid cylinder will bridge over hollow areas, the tires act independently, allowing compaction of the mat on uneven surfaces. Pneumatic rollers produce higher uniformity in density, improved surface sealing and superior aggregate orientation [1]. The spaces in between wheels provide room for the aggregate to move and reach a stable orientation.

2.3. INTELIGENT COMPACTION (IC)

In mid-1980s a compaction documentation system (CDS) was introduced in Sweden. CDS task was to keep track of rolling operation. There was no sensor used in CDS and all of the records including lane change, direction change and number of passes, beginning and the end of rolling zone were to be entered into the system by the operator [11]. Currently, according to the Federal Highway Administration (FHWA), IC is a technology which acquires real-time kinematic global positioning system (GPS), continuous compaction control (CCC) device and onboard real-time display of IC parameters to improve the compaction uniformity. IC records compaction measurements including number of roller passes, intelligent compaction measurement value (ICMV), GPS location of the roller, roller vibration parameters and surface temperature profile. Based on the information provided by the IC on the display screen, the operator can either manually, or let the IC automatically, adjust the roller operation for optimum performance. Roller pass mapping on the operator screen allows the operator to match the rolling pattern accurately and assure the compaction uniformity [12].

ICMV is the roller parameter measured to estimate the surface density. This parameter may differ for soil and asphalt and also among different manufacturers [13].

2.3.1. Monitoring Roller Location

Operating roller back and forth for hours, while at the same time keeping track of the number passes, coverages and the rolling zone limits is challenging and prone to human error. This leads to non-uniform compaction and finally causing non-uniformity in the density of the surface being compacted. To solve the issue, GPS was integrated into the IC in order to provide the operator with a real-time mapping of the roller passes on the mat. Using the map, operator can assure conformity with the roller pattern [14].

Introduction to GPS application

A global positioning system (GPS) is a system comprised of three segments: space, control and user. The space segment is a constellation with a minimum of 24 operational satellites. At least 4 operational satellites are placed in each of the 6 orbital planes. This arrangement allows 4 to 10 satellites being accessible from any place on the earth. Each satellite transmits a unique identifying signal containing its location coordinates as a function of time generated by a high precision atomic clock. The control segment of the GPS includes one master control station

(MCS) located at Schriever Air Force Base at Colorado, USA and also operational control segments (OCS) around the world. OCS units are distributed around the world in a way that each satellite can be monitored from at least two OCS simultaneously. Each satellite passes over an OCS twice a day. The OCS units monitor the satellite location and compare it with the information received from the satellite. MCS collects this information from the OCS units around the world and update the atomic clock on the satellite accordingly. Finally, the user is anyone or any object that uses a GPS antenna and a GPS receiver to find its location [15].

Once a GPS antenna is connected to at least three satellites, the receiver analyzes signals from each satellite to measure the satellite distance from the antenna location, Figure 9. Knowing the satellite locations and the distances of the desired point to each of the satellites, it is possible to find the location using the resection concept. The resection concept is a geometrical method commonly used in surveying to find a position on a map based on the grid azimuths of two or more well-defined locations.

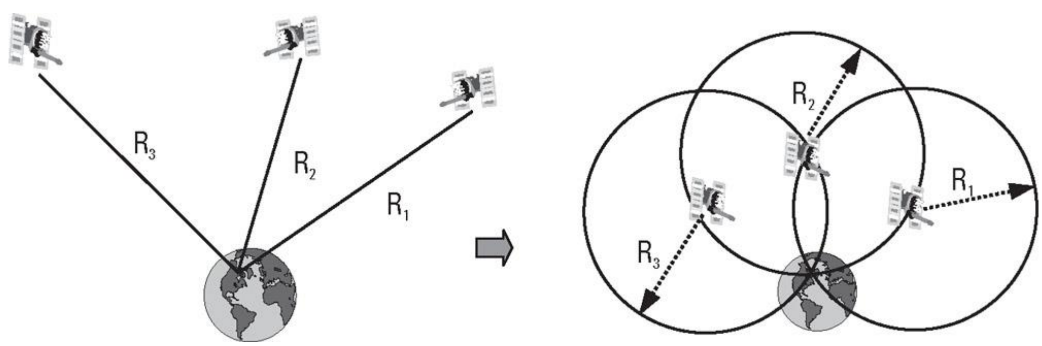

Figure 9 the Basic Idea of GPS Positioning [15]

GPS devices fall into four categories based on their precession. The “Autonomous” type includes devices with a horizontal precession tolerance around 10 to 15 meters. “DGPS” devices present a relatively higher accuracy with an error tolerance ranging from 0.5 to 4 meters. “Float” devices’ error is less than a meter. The highest level of accuracy is gained by “Fixed” type which has an error range of 1 to 3 centimeters [12].

Point positioning or autonomous positioning involves a GPS device which simultaneously tracks four or more GPS satellites to find its location, Figure 10.

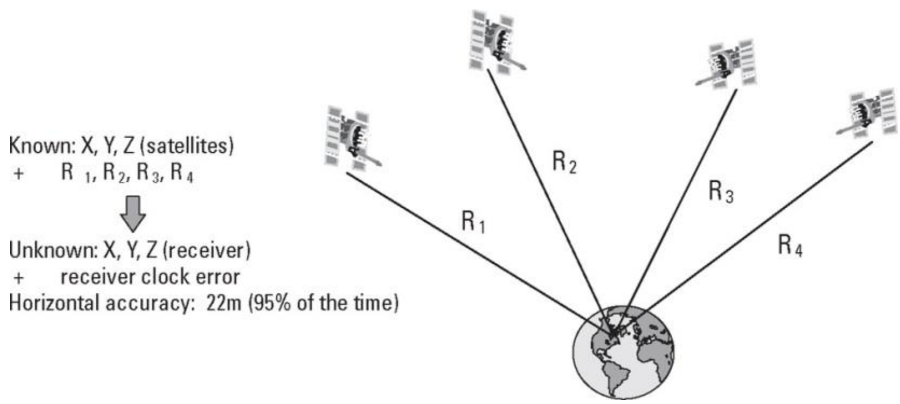

Figure 10 Autonomous Positioning [15]

Relative positioning or differential positioning is the technique used by the fixed type GPS. It involves two or more GPS receivers simultaneously tracking the same satellites to find their relative coordinates. One of the receivers serves as stationary reference fixed at a location with precisely known coordinates. The location of the other receiver known as the rover or remote receiver, is desired. The rover coordinates are determined relative to the stationary reference using measurements recorded simultaneously at the two receivers [15].

For the purpose of mapping roller passes on the mat surface, both high level of data precession and real-time positioning are required. The solution to these requirements is Real-Time Kinematic (RTK) GPS [12]. RTK is a mode of relative positioning where remote station is traveling. The positioning measurements are done in real-time, instead of gathering satellite signals for post processing in order to produce maps. Shorter signal reception time for a traveling remote station, compared to a static one, reduces the data accuracy from millimeters to few centimeters [15]. The RTK GPS operation is demonstrated in Figure 12.

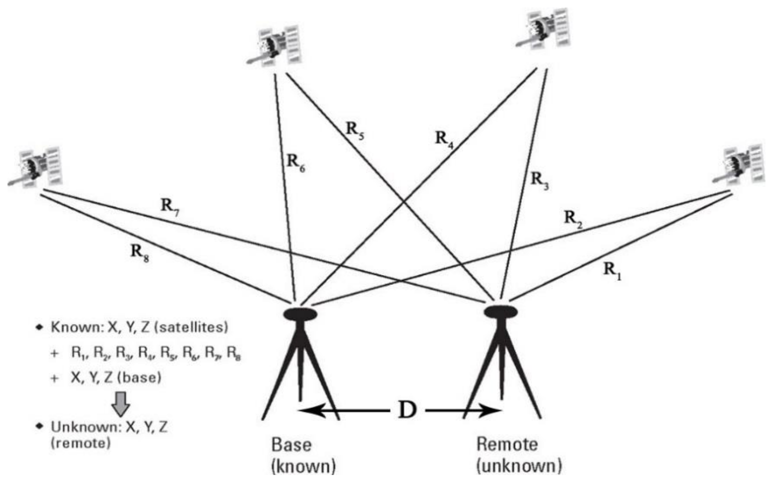

Figure 11 Relative Positioning [15]

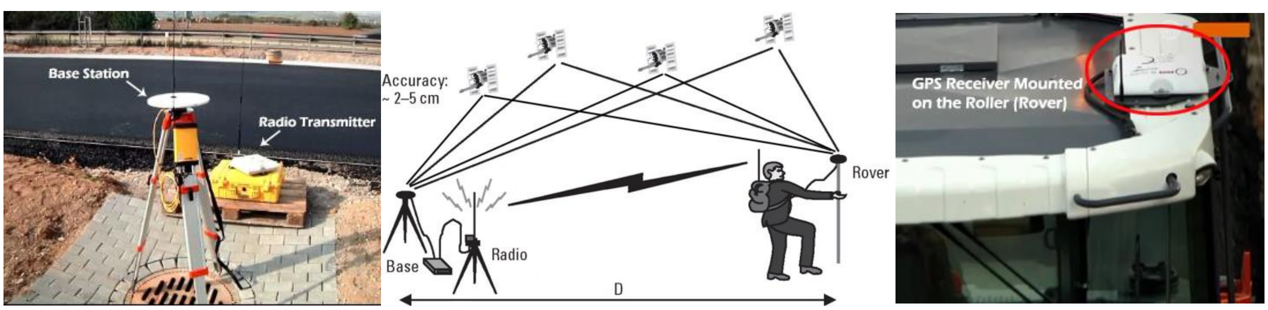

Figure 12 RTK Demonstration (HAMM), [15]

It is essential for the remote station to stay within 2 miles of the base station. Moreover, the line of the sight between the two stations must be almost obstacle free. If the connection between the two stations is lost, then the GPS configuration simply demotes to “Autonomous” mode [12].

2.3.2. Intelligent compaction for quality control

According to the US congress, in 2010 the US federal government, states and local agencies were spending about $160 billion annually on building, operation, and maintenance of roads [16]. To optimize the investments in roadways, agencies must follow their quality assurance (QA) plans. QA is referred to all of the plans and systematic actions required to assure that a material or facility will accomplish the design expectations in service. QC includes those QA tasks and considerations required to be implemented in the process of production and construction to achieve a level of quality or match specifications in the end product. The task of measuring the degree of conformity of the material or the end product with the specification is called inspection [17].

Compaction QC/QA procedures that are currently in practice, require extraction of roadway cores from the finished pavement. The major drawbacks associated with these methods include limited inspection samples (typically 1:1,000,000) and time consumption which may delay the construction. In the end, the results are the indication of the density at the test location, (not necessarily an accurate indicator of the density over the entire mat).

Horan et al, [18] studied the improvement in implementation of roller pattern by operators as a part of FHWA intelligent compaction pooled fund (ICPF) project. The roller pass mapping device was installed on a roller. The operator was not allowed to look at the screen in the initial phase. In the second phase, the operator was trained to use the information from the screen. Figure 13, compares the rolling map from the phase one and two.

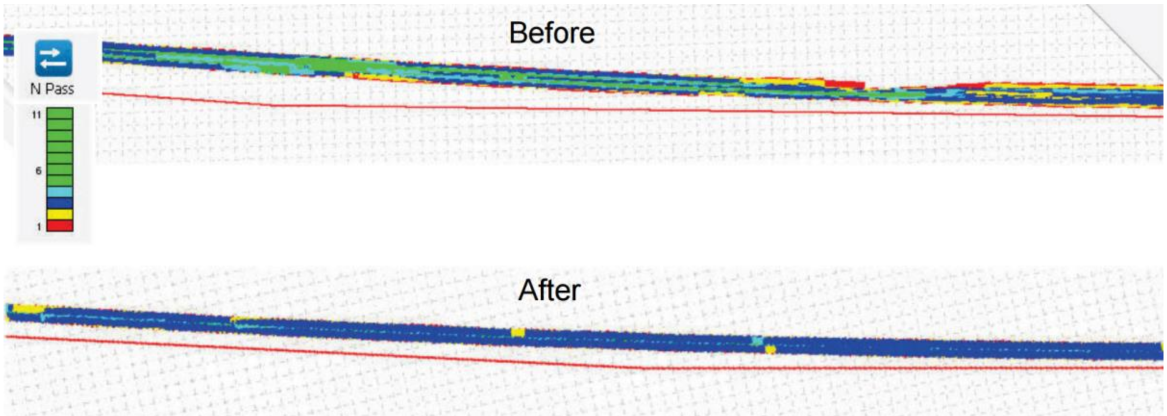

Figure 13 Improvement Observed in Implementing Roller Pattern by an Operator after Using IC [19]

The result shows considerable improvement in both uniformity and compliance with the roller pattern.

2.4. COMPUTER VISION

Developing a cost effective, accurate and self-sufficient solution for roller path mapping is analogues to research in the field of robotics and autonomous vehicles. The literature presented here discusses the science and technology used in robotics for mapping.

2.4.1. Perceiving the environment

Perception and localization often rely on each other. Building a map is constructing a presentation of the environment. Once the environment is perceived, the robot can match the information with the preset map for localization. There are also situations where the robot constructs the map and localize itself at the same time. It is called simultaneous localization and mapping (SLAM) [20]. The first step in mapping is perceiving or sensing the environment. Sensors in robotics are classified as proprioceptive and exteroceptive. Proprioceptive sensors provide information about internal state of the machine such as the position of the wheels. The exteroceptive sensors acquire information from the surrounding environment such as the spatial information or the colors [21]. In the following, some of the most popular sensors used in robotics are briefly discussed:

Machine Control Sensors

The machine control sensors are proprioceptive sensors that are commercially available and provide a wide range of data such as machine drive parameters, distance traveled, speed and orientation. A combination of this information can be used to track the equipment [22].

Dead Reckoning Sensors

Dead reckoning (DR) is the process that uses parameters such as estimated speed, elapsed time and direction to calculate the current location of an object based on a previously known position. These type of sensors are generally classified as proprioceptive sensors. DR is susceptible to accumulated error. Odometers and inertial navigation systems are instances of DR. Odometer is a device that measures the distance traveled by a moving object. In a common means of odometry, the distance is measured based on the number of axle's revolutions and known diameter of wheels [23]. Inertial navigation systems (INS) use gyroscope to measure angular rate data and accelerometer for velocity rate information. INS is a self-contained, non-radiating, non-jammable, dead reckoning navigation system which provides dynamic tracking information through direct measurements. The problem associated with INS is time and distance accumulated error. One solution to this issue is to frequently reset the INS error by tying its measurements to some known locations [24]. Ultimately the major application of INS is in the areas where other absolute positioning systems such as GPS signal reception maybe lost for a short period of time. Barshan and Whyte (1995) used an INS system comprised of a gyroscope, an accelerometer and two tilt sensors in a radar navigated cargo truck. The results showed INS positioning is accurately reliable for about 10 minutes. In addition to accuracy degradation with time and distance, the system is highly susceptible to vibration and its reliability duration time may drop to few seconds if the system is on vibration [24]. This shortcoming makes INS totally improper for using on vibrating rollers.

In general dead reckoning methods have many advantages including simplicity, low cost and most importantly they do not rely on an external source for functionality. However their biggest issue is the accumulated error. Therefore, they are commonly used as the backup navigation mechanism.

Time of Flight Based Sensors

Time of flight (ToF) based measurement sensors such as LiDAR (light radar), SONAR (sound navigation and ranging) and radar have also been used in robotics for both mapping and navigating. ToF includes a variety of methods that calculate the travel time of an object, wave, light, particle or electromagnetic radiations trough a medium. LiDAR is a laser range finder that measures distance by illuminating at a target object with a laser and analyzing the reflected light. SONAR is a sound propagation range sensing that was initially developed for submarine applications. SONAR systems vary based on the sonic wave frequency from infrasonic to ultrasonic. SONAR is also available for airborne applications which are called SODAR (Sonic Detection and Ranging). By nature, SODAR is similar to RADAR (Radio Detection and Ranging) system but use sonic waves instead of radio waves for detection.

Global Positioning System

GPS is perhaps the most popular methods for mapping. GPS has been discussed in this chapter, earlier.

Ultra-Wideband Sensors

UWB is a radio based positioning technology which can detect and track objects in limited areas. The system consists of a network of UWB receivers, UWB tags and a data processing unit. The tag(s) on the moving object transmits low energy radio waves. These signals are then received by UWB receivers and being analyzed to find the location of the tag(s). Each signal contains four pieces of information having two of them will be enough to locate the tag [22]. This technology offers reliable spatiotemporal data in tracking resources on construction site [25]. However the biggest shortcoming of this technology is the requirement of a wired network of sensors installed all around the site. This requirement makes UWB application impractical for temporary and linear projects such as highway construction [22].

Radio Frequency Identification (RFID)

RFID is a wireless system that identifies and tracks a tag through radio frequency electromagnetic fields. The system consists of a tag which is an electronic chip containing identification information and a reader that reads the information stored on the tag and transfer them to a host computer. The biggest advantage of RFID is that it does not require a direct line of site for communication. Moreover RFID tags are very durable and can be encapsulated.

RFID has been used in for a variety of purposes in construction projects such as monitoring loading, hauling and delivery times for trucks. The RFID reader identifies and checks in an object carrying a tag while entering to the loading station. Another reader installed at the exit gate identifies and checks out the same objects. This is how the system measures loading time for each truck. Likewise, truck travel times, onsite delays and so on can be measured [26]. As it can be inferred from the example above a tag can be detected only if it is placed in the reader vicinity. Therefore this technology can be used for tracking objects at stations and not for continuous tracking of an object.

Vision Based Methods

Images are detailed, accurate and compact sources for automated data collection [27]. Development of cheap digital cameras and high capacity storage devices has made images and videos great means for progress measurement, claim reports, safety and training on construction sites [22]. Computer vision (CV) is defined as the field of techniques for acquiring, processing, analyzing, and understanding images and, in general, high-dimensional data from the real world in order to produce numerical or symbolic information. A general idea in development of this area has been to mimic the ability of human vision by electronically perceiving and understanding of a scene [28]. In terms of application in construction field, CV has become quite popular as it provides the opportunity to collect a vast amount of data from site videos and images. For instance, CV has been used in construction progress monitoring, defect detection, automated image retrieval and productivity measurements [22]. Some other instances of using CV in civil engineering includes pavement distress surveying [29], health monitoring of structures [30], strain measurement of loaded samples [31], structural assessment of underground pipes [32], movement of sediment particles [33] and many more.

With regards to vision perception, currently three major categories including monocular, omnidirectional and stereo vision systems are available. Both monocular and omnidirectional vision systems have a single camera whereas the stereo vision systems use two cameras. The omnidirectional and monocular systems can only generate 2D information. In monocular systems the camera is placed horizontally which results in a view field less than 180 degrees. In omnidirectional vision systems, to achieve a 360 degree field of view, the camera is mounted vertically pointed upward at a convex mirror [34]. Compared to monocular images, the retrieved images by omnidirectional cameras have lower resolution. On the other hand, the stereo vision systems are inspired by human vision and use a pair of images from two specially mounted cameras to perceive the world in 3D [35].

Monocular vision is mainly used for landmark recognition. Landmarks are environmental features that are familiar to the machine and will be used as navigational aids. Once a land mark is detected the machine will be able to approximate its current location. This approach is called selective visual attention landmark recognition (SVALR) and is frequently used in vision based autonomous robots [36]. Vision based robots' architecture consists of five essential components:

- **Maps**: The system needs some internal knowledge of the surrounding environment in order to perform tasks. A sequence of images can be used to automatically generate a 2D CAD geometric representation of the machine path.
- **Data Acquisition**: The system captures the surrounding environment using a camera.

- **Feature extraction**: Significant features such as edges, texture and colors can extracted from images.
- **Land mark recognition**: The system looks for matches between the extracted features and the expected landmarks based on the predefined criteria.
- **Self-localization**: The self-localization algorithm calculates the robot's current position relative to the detected land mark and its earlier position in real time.

2.4.2. Image processing

Image processing which normally refers to digital image processing is the process of analyzing digital images or video frames using a computer to produce either manipulated images or extracting a set of desired characteristics or parameters. Image processing can be used wherever visual information are needed. Examples of image processing applications are in quality control for counting particles and measuring the size distribution, in many medical diagnosing such as tomography, exploring dynamic processes such as plant growth in botany, in climatology to study the cloud patterns and so on [37]. In CV, image processing is used for feature extraction. Some of the popular techniques and tools used in image processing for feature extraction are discussed in the following:

Edge Detection

In processing images, an edge is a collection of points where an abrupt change in pixels' intensity occurs. Therefore, edges can be detected by taking partial derivatives from an image function with regard to x and y axes. In other words, a change in the image function can be described by a gradient that points toward the largest growth. To detect an edge, the behavior of the image function is investigated within the neighborhood of the target pixel. An edge is a vector variable with magnitude and direction components.

Various different operators including: Roberts, Laplace, Prewitt, Sobel, Robinson and Kirsch have been used for edge detection. The Roberts operator is very simple and easy since it only investigate a 2x2 pixel neighborhood for edge. The Laplace operator is very popular and uses second derivative. Therefore, it is only based on magnitude and not direction. Prewitt operator uses the first derivative and estimates the gradient in different directions to find the greatest magnitude. Sobel operator is often used to estimates edges in horizontal and vertical directions [38].

Canny [39] introduced a computational approach to edge detection, Figure 14. The algorithm is optimal for step edges. The performance of the detector depends on detection criterion, localization criterion and one response criterion. Detection criterion determine which edges are important. Localization criterion minimizes the distance between the actual and the detected edge. Lastly, the one response criterion determines a unique response to the detected edge. Canny algorithm uses Laplace operator which is based magnitude and not direction.

Figure 14 Canny Edge Detection at Two Different Scales [38]

Harris Corner Detector

Typical features in an image usually include edges, corners (intersect points) and blobs (region of interest). Corners have specific characteristic that makes them easy to detect in an image. A corner is the intersection of two edges where the gradient of the image changes in two directions at that point. Therefore, corners are typically used as features in CV. In 1988, Harris and Stephens proposed an algorithm to detect corners in an image based on the property described in the above [40]. The so called Harris corner detector sweeps a window *W*(x,y) (with displacements *u* in the x direction and υ in the Y direction) within the grayscale image "I" and will calculate the variation of intensity from Equation 1:

$$E(u,v) = \sum_{x,y} w(x,y)[I(x+u,y+v) - I(x,y)]^2 \qquad \text{Equation 1}$$

Where

W(x,y) is the window at position (x,y)

I(x,y) is the intensity at (x,y)

I(x+u,y+v) is the intensity at the moved window (x+u,y+v)

Since the goal is to find the windows with large variation in intensity. Thus, the following term in Equation 1 has to be maximized:

$$\sum_{x,y}[I(x+u,y+v)-I(x,y)]^2$$

Using Tylor expansion:

$$E(u,v)\approx\sum_{x,y}[I(x,y)+uI_x+vI_y-I(x,y)]^2\approx\sum_{x,y}u^2{I_x}^2+v^2{I_y}^2+2uvI_xI_y$$

Which could be expressed in matrix form:

$$E(u,v)\approx[u \quad v]\left(\sum_{x,y}w(x,y)\begin{bmatrix}I_x^2 & I_xI_y\\ I_xI_y & I_y^2\end{bmatrix}\right)\begin{bmatrix}u\\ v\end{bmatrix}$$

If

$$M=\sum_{x,y}w(x,y)\begin{bmatrix}I_x^2 & I_xI_y\\ I_xI_y & I_y^2\end{bmatrix}$$

Then

$$E(u,v)=[u \quad v]M\begin{bmatrix}u\\ v\end{bmatrix}$$

The chance of an edge occurring within a window is evaluated with R, where:

$$R=\det(M)-k(trace(M))^2$$

If R is greater than a threshold then the window contains a corner.

Line Detection

Once an edge is detected, it represents a series of points. Many times, further information such as a particular shape or an equation that determines the edge is desirable. There are different algorithms that try to find a particular shape or patterns in an image. The simplest and most common ones are used for straight line detection. To find a straight lane in an image, there are different techniques including:

- Least Square Fit: It is a mathematical procedure that finds the best-fitting line to a given set of points by minimizing the sum of the squares of the offsets ("the residuals") of the points from the fitted line.
- Random Sample Consensus (RANSAC): It is an iterative method to estimate the slope and intercept from a set of observed data which contains outliers. The algorithm finds the line parameters that maximize the inliers and minimize the outliers.
- Hough Transform: It is both a segmentation and line fitting tool that can be used to find objects including straight lines in a scene [39]. To avoid the problem of dealing with vertical lines where the slope approaches infinity, the Hough transformation uses polar coordinate system. In general, for each point (x_0,y_0) in Cartesian coordinate the polar coordinate transformation is described by

$$r_\theta = x_0 \cos\theta + y_0 \sin\theta \qquad \text{Equation 2}$$

Where "r" and "θ" represent each line that passes through (x_0, y_0). If for a given (x_0, y_0), "r" is plotted versus "θ" for the family of the lines passing through (x_0, y_0), the result will be a sinusoid shape. If such plots are created for a series of points, the "r" and "θ" designated by the point where the sinusoid plots cross, describes a line that passes through the points whose plot crossed, see Figure 15.

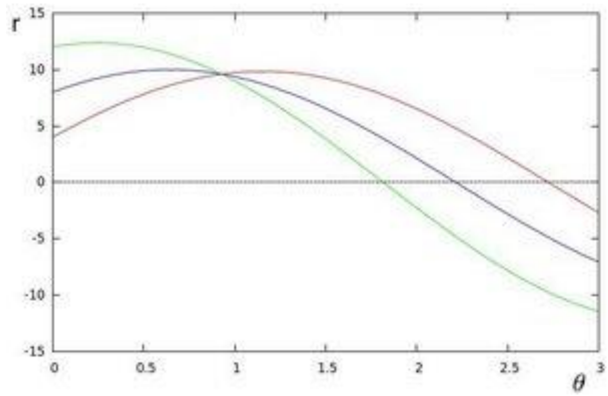

Figure 15 Illustration of Hough Transform

Segmentation

Segmentation divides an image into regions where there are a strong correlation with the objects or areas of the real world captured in the image. There are complete and partial segmentation. In complete segmentation, the problem is looking for contrasted objects plotted on a uniform background. In partial segmentation, the image is divided into separate homogeneous regions based on a sectioning criterion such as brightness, color, reflectivity, texture, etc [38].

Region of Interest

Region of interest (ROI) is a technique that saves time and increases the productivity of the computation process by only analyzing that part of image that contain useful information [38].

2.4.3. Image Registration

Image registration is the method of aligning a series of images of the same scene. The method involves defining one image as the reference and finding the geometric transformations that allow aligning other images with the reference. For the one-dimensional case shown in Figure 16:

$$G(x) = F(x + h)$$

Since

$$F'(x) = \frac{F(x + h) - F(x)}{h} = \frac{G(x) - F(x)}{h}$$

Therefore:

$$h = \frac{G(x) - F(x)}{F'(x)}$$

Lucas and Kanade 1981, optimized and generalized the above transformation function and found Equation 3 [41]:

$$h \approx \left[\sum_x \left(\frac{\partial fF}{\partial x}\right)^T [G(x) - F(x)]\right] \left[\sum_x \left(\frac{\partial fF}{\partial x}\right)^T \left(\frac{\partial fF}{\partial x}\right)\right]^{-1} \qquad \text{Equation 3}$$

For two-dimensional cases such translation would be calculated along both x, y directions.

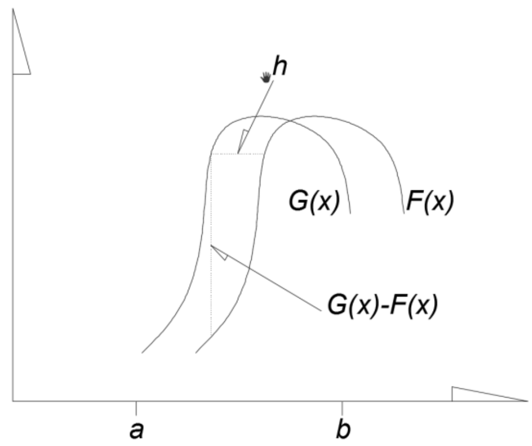

Figure 16 one-dimensional translation for image registration

2.4.4. Simultaneous localization and mapping

Simultaneous localization and mapping (SLAM), is the method used by mobile robots placed in an unknown environment to incrementally construct a consistent map of this environment and simultaneously marking its location on the map being developed [42]. SLAM consists of multiple parts; Landmark extraction, data association, state estimation, state update and landmark update. The formulation of the SLAM problem and the solution are discussed in the following:

SLAM problem

Figure 17 shows a mobile device moving through an environment and taking relative observations of a number of unknown landmarks using a sensor attached to the device.

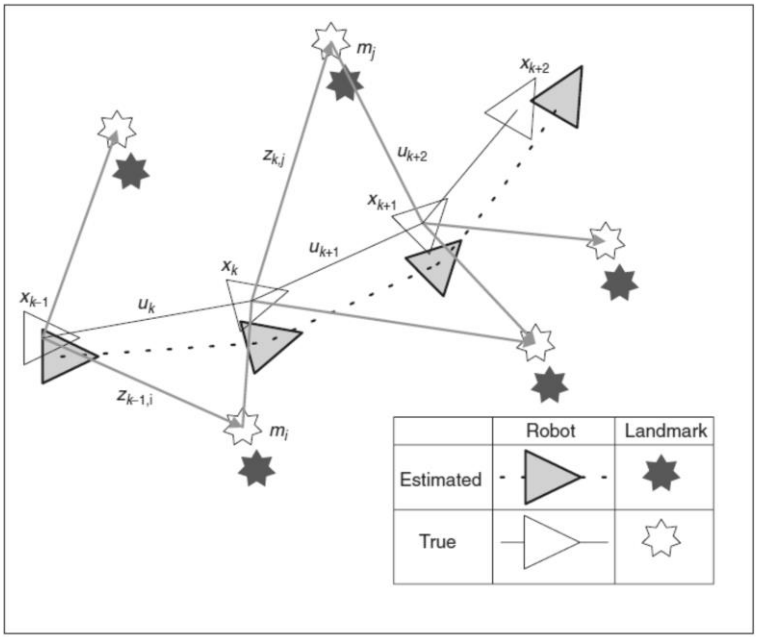

Figure 17 SLAM Problem [42]

In Figure 17:

x_k : The state vector describing the location and orientation of the mobile device

u_k : The transit vector, applied at time $k - 1$ to transfer the mobile device to a state x_k at time k.

m_i : Vector describing the location of the *ith* landmark whose true location is assumed time invariant

z_{ik} : An observation of the location of the ith landmark, taken from the mobile device at time k. If there are multiple landmark observations at any one time or when the specific landmark is not relevant to the discussion, the observation will be written simply as z_k

The history of data is also recorded in form of series:

$\mathbf{X}_{0:k} = \{\mathbf{x}_0, \mathbf{x}_1, \cdots, \mathbf{x}_k\} = \{\mathbf{X}_{0:k-1}, \mathbf{x}_k\}$

$\mathbf{U}_{0:k} = \{\mathbf{u}_1, \mathbf{u}_2, \cdots, \mathbf{u}_k\} = \{\mathbf{U}_{0:k-1}, \mathbf{u}_k\}$

$\mathbf{m} = \{\mathbf{m}_1, \mathbf{m}_2, \cdots, \mathbf{m}_n\}$

$\mathbf{Z}_{0:k} = \{\mathbf{z}_1, \mathbf{z}_2, \cdots, \mathbf{z}_k\} = \{\mathbf{Z}_{0:k-1}, \mathbf{z}_k\}$

Probabilistic SLAM

In the probabilistic form of SLAM, the probability distribution of $P(x_k, m|Z_{0:k}, U_{0:k}, x_0)$ must be computed for all times *k*. The process can start with an estimate for the distribution of

$P(x_{k-1}, m|Z_{0:k-1}, U_{0:k-1})$ at time *k-1*, the joint posterior and the next system state u_k and observation z_k are computed using the Bayes' theorem. To perform the analysis, a state transition model and an observation model are defined. The observation or the measurement model $P(\mathbf{z}_k|\mathbf{x}_k, \mathbf{m})$ describes the probability of making an observation $\mathbf{z}_k$ with known location of the mobile device and the landmark. The motion or the transition model $P(\mathbf{x}_k|\mathbf{x}_{k-1}, \mathbf{u}_k)$ describes the change in the system state [42].

The formulated probabilistic SLAM problem is a standard two-step recursive (sequential) estimation (time-update) presented in Equation 4 and correction (measurement-update) by Equation 5.

<u>System state based on time-update</u>

$$P(\boldsymbol{x}_k, \boldsymbol{m}|\boldsymbol{Z}_{0:k-1}, \boldsymbol{U}_{0:k}, \boldsymbol{x}_0) = \int P(\boldsymbol{x}_k|\boldsymbol{x}_{k-1}, \boldsymbol{U}_k) \times P(\boldsymbol{x}_{k-1}, \boldsymbol{m}|\boldsymbol{Z}_{0:k-1}, \boldsymbol{U}_{0:k-1}, \boldsymbol{x}_0) dx_{k-1} \qquad \text{Equation 4}$$

<u>Measurement update</u>

$$P(\boldsymbol{x}_k, \boldsymbol{m}|\boldsymbol{Z}_{0:k}, \boldsymbol{U}_{0:k}, \boldsymbol{x}_0) = \frac{P(z_k|x_k, m)P(\boldsymbol{x}_k, \boldsymbol{m}|\boldsymbol{Z}_{0:k-1}, \boldsymbol{U}_{0:k}, \boldsymbol{x}_0)}{P(\boldsymbol{z}_k|\boldsymbol{Z}_{0:k-1}, \boldsymbol{U}_{0:k})} \qquad \text{Equation 5}$$

Solutions to the SLAM Problem

Solutions to the SLAM problem must provide appropriate presentation for both observation and motion models, efficient computation of prior and posterior distributions. So far the best solution is provided by extended Kalman filter (EKF). The extended Kalman filter (EKF) is the heart of SLAM process [42].

Kalman filter (KF) is an optimal linear estimator. KF consists of an algorithm for recursively estimating the state of a dynamic system from noisy measurements. The filter combines all available measured data, plus any prior knowledge about the system and the measuring devices to make an estimate of the variable of interest with minimized statistical error [20]. To illustrate the KF algorithm, assume a measurement describing the system state partially or entirely is available at least on an intermittent basis. The current and the last system state or measurements are denoted with time t_k and t_{k-1}. x and z are system state and measurement. For a linear system:

$$\begin{cases} \underline{\hat{x}}_{k+1} = \varphi_k \underline{\hat{x}}_k + G_k \underline{w}_k \\ \underline{z}_k = H_k \underline{x}_k + \underline{v}_k \end{cases} \qquad \text{Equation 6}$$

Where:

$\underline{\hat{x}}_k$= State vector estimate at time t_k
Φ_k = Transition matrix (relates $\underline{x}_k$ to $\underline{x}_{k+1}$)
G_k = Process noise distribution matrix (transforms the $\underline{w}_k$ vector into the coordinates of $\underline{x}_k$)
$\underline{w}_k$= Disturbance sequence or process noise sequence

z_k = Measurement at the time t_k

H_k= Measurement matrix or observation matrix (relates $\underline{x}_k$ to $\underline{z}_k$ in the absence of measurement noise)

$\underline{v}_k$= Measurement noise sequence

Kalman filter equations for a linear system are as follows:

$$System\ Model \begin{cases} \hat{\underline{x}}_{k+1} = \varphi_k \hat{\underline{x}}_k & Predict\ State \\ P_{k+1} = \Phi_k P_k\ \Phi_K^T + G_k Q_k G_k^T & Predict\ Covariance \end{cases} \quad \text{Equation 7}$$

$$Kalman\ Filter \begin{cases} K_k = P_k^- H_k^T [H_k P_k^- H_k^T + R_k]^{-1} & compute\ Kalman\ gains \\ \hat{\underline{x}}_k^+ = \hat{\underline{x}}_k^- + K_k [\underline{z}_k - H_k \hat{\underline{x}}_k^-] & update\ state\ estimate \\ P_k^+ = [1 - K_k H_k] P_k^- & update\ its\ covariance \end{cases} \quad \text{Equation 8}$$

Where Q_k is the matrix describing the uncertainty in the system, whereas the R_k matrix models the uncertainty associated with measurements. The developer must develop these matrices based on knowledge of the system and sensors.

Figure 18, displays the KF algorithm. The linear model is split into two groups, the system model and the KF. The system model and KF do not run at the same time. The system model runs at high frequency to report the system state with time. The system model proceeds solely based on time measurements. On the other hand the KF runs when measurements are a both available and acceptable. In that case KF runs after the state has been predicted by the system for that cycle [20].

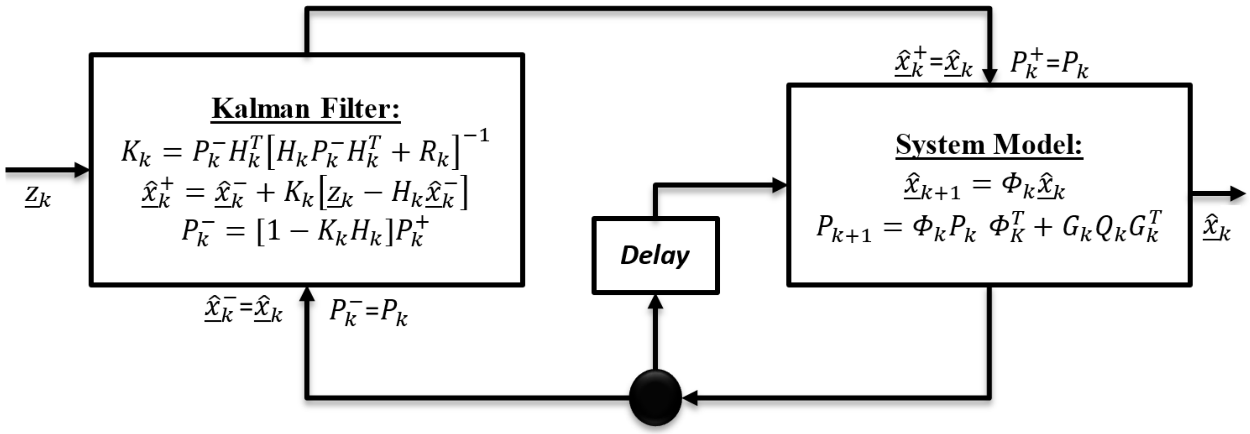

Figure 18 KF Algorithm

Extended Kalman filter (EKF) deals with non-linear motion and observation models [42]. Equation 9 shows the general model for non-linear system state and observation.

$$\begin{cases} \dot{\underline{x}} = \underline{f}\left(\underline{x}, t\right) + \underline{g}(\underline{w}, t) \\ \underline{z} = \underline{h}\left(\underline{x}, t\right) + v(t) \end{cases} \qquad \text{Equation 9}$$

Where:

f, *g* and *h* are vector valued non-linear functions

w and *v* are noises

Equation 9 is used to develop the EKF form the KF presented in Equation 7 and Equation 8. In the EKF, the trajectory error estimates are used to update the reference trajectory with time. Equation 10 and Equation 11 describe the EKF [20].

$$System\ Model \begin{cases} \hat{\underline{x}}_{k+1} = \varphi_k \hat{\underline{x}}_k & Predict\ State \\ P_{k+1} = \Phi_k P_k\ \Phi_K^T + G_k Q_k G_k^T & Predict\ Covariance \end{cases} \qquad \text{Equation 10}$$

$$Kalman\ Filter \begin{cases} K_k = P_k^- H_k^T [H_k P_k^- H_k^T + R_k]^{-1} & compute\ Kalman\ gains \\ \underline{\hat{x}}_k^+ = \underline{\hat{x}}_k^- + K_k \left[\underline{z}_k - h(\underline{\hat{x}}_k^-)\right] & update\ state\ estimate \\ P_k^+ = [1 - K_k H_k] P_k^- & update\ its\ covariance \end{cases} \quad \text{Equation 11}$$

VSLAM

In the past, SONAR and laser rangefinders have widely and successfully been utilized for simultaneous localization and mapping [43], [44], [45]. In recent years with the development of image sensors and cheap cameras which are compact, accurate and non-invasive, vision has become more popular for SLAM. Research studies in the field of visual SLAM (VSLAM) can be categorized by stereovision, monocular vision, off-line SLAM and real-time SLAM.

Structure from Motion (SfM) builds the 3D structure of a scene and the camera parameters from a bundle of images from that scene, taken from different view point. SfM in nature is an offline method which requires analyzing a complete image sequence to create a reconstruction of the camera trajectory and scene structure. Hence, SfM cannot be used for real-time SLAM [45]. McLauchlan and Murray [46] worked on Variable State-Dimension Filter (VSDF) for simultaneous structure and motion recovery from a moving camera by utilizing a sparse information filter framework. VSDF is not accurate for long term tracking and fails loop closing [45]. The major part of published literature on VSLAM focuses on stereo vision application. Despite the considerable uncertainty in the depth information provided by the stereo vision and the complexity involved in the calibration, yet it has demonstrated the most accurate results in long run, compared to the other visual configurations [47]. The most complicated problem in VSLAM is real-time 3D application using monocular vision or single camera. Single camera is easy to use but have the problem of scale ambiguity. Davison [48] tackled this problem and developed a solution called MonoSLAM which is a real time single camera SLAM with the emphasis on the localization [45].

Visual Odometry

Visual odometry or egomotion is the estimation of camera motion. Egomotion is usually the base for recovering the motion and structure in monocular setting. Generally, there are two approaches toward egomotion, feature matching between consecutive frames and tracking features over stack of frames. The earlier method suffers from higher drift rates since it is based on the data from only two images. The feature track over a sequence of frames results in higher accuracy but requires higher computational capacity. To solve this issue a bundle adjustment algorithm that optimize the analysis over a limited number of images is applied. Some other algorithms also use GPS or INS data to reduce the drift [49]. For on road applications with a single camera pointed downward, a planer vision is analyzed which results in reduced degrees of freedom for camera motion estimation and provides improved results. Kitt et al, [49] proposed an algorithm for egomotion estimation solely from monocular image stack. The algorithm reduces the degrees of freedom with the assumption of planarity for the road surface and fixed camera hight. The results shows no significant drift from the true path. Lovegrove et al, [50] used a rear parking camera for visual odometry and demonstrated results close to the ground truth path. He also improved the system accuracy by fusing the visual odometry with GPS.

2.4.5. Camera Calibration

The calibration process is required to determine intrinsic and/or extrinsic parameters of a camera. Intrinsic parameters are specific to a camera. It includes information such as focal length (f_x,f_y), optical centers (c_x,c_y), scaling factors for row and column pixels, Skew factor, Lens distortion (pin-cushion effect) parameters. Given a set of images taken using the camera, there are mathematical solutions available that allow obtaining the camera parameters [51].

Mathematical Solution

The configuration of a camera matrix is described in Equation 12. To find the calibration coefficients, Equation 13 and Equation 14 must be solved.

$$Camera\ Matrix = \begin{bmatrix} f_x & 0 & c_x \\ 0 & f_y & c_y \\ 0 & 0 & 1 \end{bmatrix} \qquad \text{Equation 12}$$

$$\begin{cases} x_{corrected} = x(1 + k_1 r^2 + k_2 r^4 + k_3 r^6) \\ y_{corrected} = y(1 + k_1 r^2 + k_2 r^4 + k_3 r^6) \end{cases} \qquad \text{Equation 13}$$

$$\begin{cases} x_{corrected} = x + [2p_1 xy + p_2(r^2 + 2x^2)] \\ y_{corrected} = y + [p_1(r^2 + 2y^2) + 2p_2 xy] \end{cases} \qquad \text{Equation 14}$$

Where

k_1, k_2, k_3 are radial distortion coefficients

p_1 *and* p_2 are tangential distortion coefficients

Calculation of these parameters is done through basic geometrical equations. The equations used depend on the chosen calibrating objects. Checkerboard is the most common calibration pattern. Calibration pattern provides a series of real word points with known relative coordinates to solve the above equations. As shown in Figure 19, the key points on a chessboard are easily detectable using corner detection algorithms.

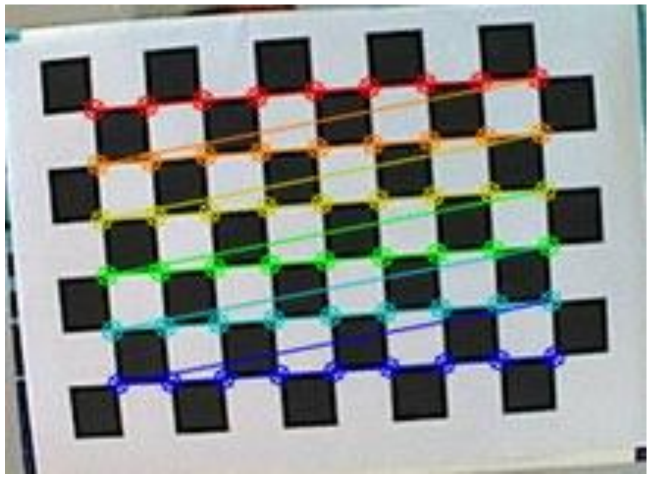

Figure 19 Keypoints Detection for a Chessboard Pattern

Once the key points are detected, their coordinates in the image system can be recovered. Knowing the size of the squares and the number of rows and columns on the board, the relative coordinate of each key point can be calculated. In theory, calibration can be done with as few as two proper captures of the pattern. However, for proper results the OpenCV manual recommends a minimum of 10 shots of a pattern from different angles, as illustrated in Figure 20. To evaluate the calibration process, a re-projection error is calculated to provide a qualitative measure of accuracy of the results. The re-projection error is the distance between the pattern key points detected in a calibration image, and the corresponding real world points projected into the same image. Therefore, a smaller re-projection error describes more accurate results. However, many camera calibration tutorials such as the one provided in Practical OpenCV book [52] recommend values less than 0.5 for satisfactory results. Zhang provided the mathematical solution of calibration [51] and the calculation of re-projection is described by R. Hartley and A. Zisserman in [53].

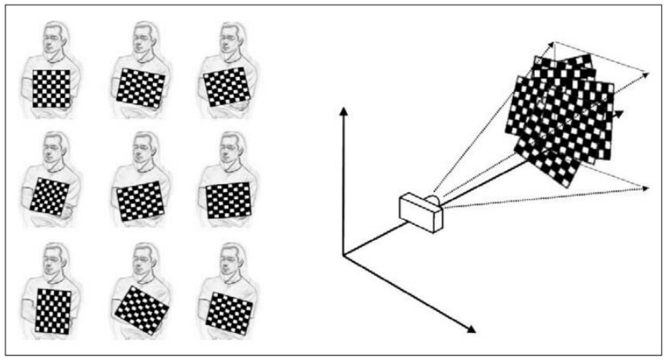

Figure 20 Using Checker Board for Calibration [54]

Extrinsic parameters corresponds to rotation and translation vectors which transforms a coordinates of a 3D point in real world to the camera coordinate system, see Figure 21.

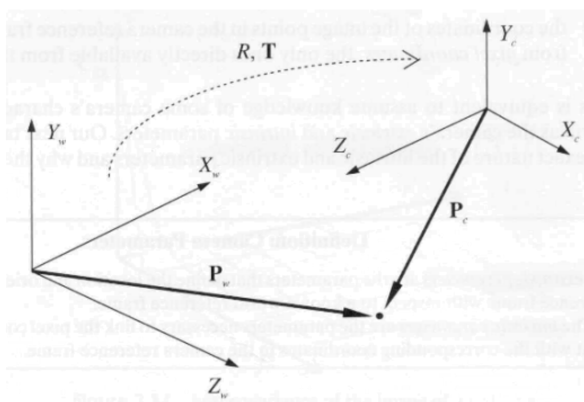

Figure 21 Transformation using extrinsic camera parameters

The extrinsic camera parameters explain the relation between the coordinates of a point P in world (P_w) and camera (P_c) coordinates. The transformation using the extrinsic camera parameters is described in Equation 15.

$$P_c = R(P_w - T)$$

Where: $R = \begin{bmatrix} r_{11} & r_{12} & r_{13} \\ r_{21} & r_{22} & r_{23} \\ r_{31} & r_{32} & r_{33} \end{bmatrix}$ is the rotation matrix and $T = \begin{bmatrix} T_x \\ T_y \\ T_z \end{bmatrix}$ is the translation matrix

If $P_c = \begin{bmatrix} X_c \\ Y_c \\ Z_c \end{bmatrix}$ and $P_w = \begin{bmatrix} X_w \\ Y_w \\ Z_w \end{bmatrix}$, then:

$$\begin{bmatrix} X_c \\ Y_c \\ Z_c \end{bmatrix} = \begin{bmatrix} r_{11} & r_{12} & r_{13} \\ r_{21} & r_{22} & r_{23} \\ r_{31} & r_{32} & r_{33} \end{bmatrix} \begin{bmatrix} X_w - & T_x \\ Y_w - & T_y \\ Z_w - & T_z \end{bmatrix}$$ Equation 15

IR Camera Calibration

Due to the physical characteristics of the IR acquisition process, accurate localization of the calibration features is generally not as easy as the optical process, subsequently causing unsatisfying calibration results. Review of the literature in this area indicates that using a heated chessboard pattern alone, and the same calibration algorithm as used for optical cameras will result in projection error greater than 1 [55].

To improve the calibration quality for IR cameras, innovative methods were found in the literature including using additional sensors such as a laser range finder [56], or using an ellipse algorithm [55] which claim to be able to reduce the re-projection error IR cameras close to 0.5 or less which are typically recommended for calibration with optical cameras.

Ellmauthaler et al. [55] method for calibration of IR camera, included developing a calibration pattern similar to conventional checkerboard consisting of miniature light-bulbs. Their algorithm fits an ellipse to the heat radiation from each light bulb and calculates the center of mass of the extracted ellipsoidal region as the starting calibration point. The center of mass pattern is later refined iteratively by modifying mappings to and from an undistorted grid model. The result of such processing chain significantly reduces the projection error when compared to the result of typical calibration algorithms used for optical cameras.

Chapter 3: **RESEARCH METHODOLOGY**

3.1. INTRODUCTION

Despite the importance of roller pass mapping, this tool has not become popular among the contractors, yet. Part of the contractors' reticence to implement the technology is related to the high cost of acquisition and the requirement for setting up a base station on the site. Therefore to overcome those issues, in this study, a self-contained device that is capable of producing roller pass maps with acceptable accuracy and affordability was developed. In this chapter the hardware selection, the mathematical approach and software development are individually discussed.

3.2. RESEARCH APPROACH

A roller pass mapping system is not a control system, the system only monitors the operation and provides information to assist the operator. Thus, a solution based on three main steps including:

1. Sensing the environment
2. Interpreting the collected data to find the roller's relative location
3. Updating the tracking map

In development of the new roller pass mapping device, different technologies were studied. The candidate methods were rated based on practicality, simplicity and cost effectiveness in achieving the objectives of this research. Figure 22 describes the overall approach used in this study.

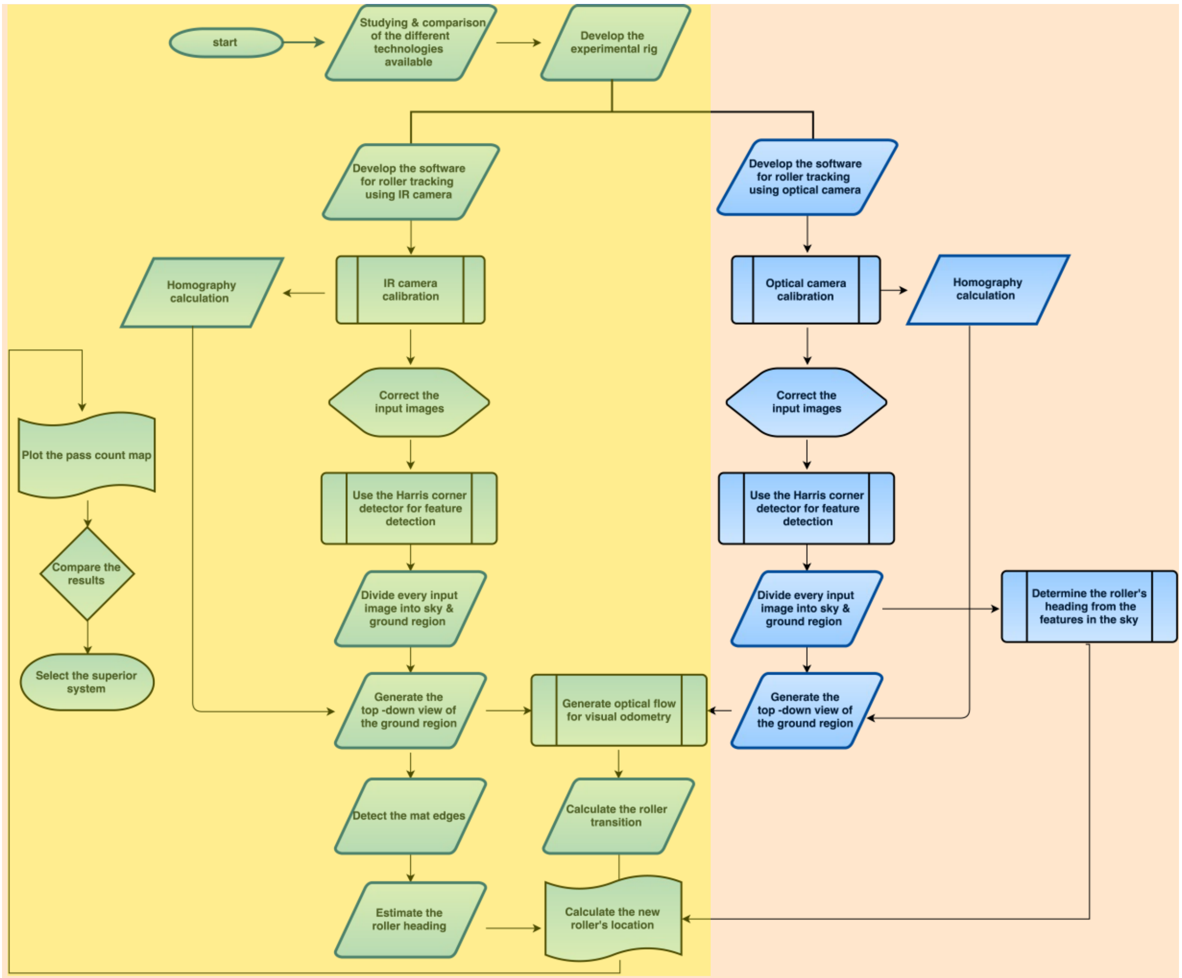

Figure 22 Research approach diagram

The highlighted part in Figure 22, describes the approach that produced better results for the purpose of this study.

3.2.1. Sensing the Environment

Based on the literature review, different technologies including machine control sensors, GPS, ultra-wideband (UWB), radio frequency identification (RFID) and computer vision based techniques have been used for automated data collection during construction. Table 1, summarizes the advantages and disadvantages of such methods.

Table 1 Comparison of Tracking Technologies

	Major Advantage	Major Disadvantage
Machine Control Sensors	Low cost, do not rely on external sources	Provide limited information of the surrounding environment
Dead Reckoning Sensors	Low cost, do not rely on external sources	Accuracy drops with time and distance, Susceptibility to vibration
Time of Flight Based Sensors	Accurate range measurement	Incapable of spectral measurements
Global Positioning System	Accuracy	Expensive for high precision applications,
Ultra-Wideband	Reliable tracking data	Requires a network around the construction site
Radio Frequency Identification	Low cost	Low range
Computer Vision	Low cost, Spectral measurement	Accumulated error for tracking

The comparison based on Table 1 led to choose computer vision for this research. An inertial sensor could be used as a backup system.

3.2.2. Hardware Selection

In the early stages of the experimental work, it became clear that data collection using an optical camera will not be effective for works performed during night. Therefore, it was decided to use an IR camera for data collection. The reasoning behind this decision relies in the nature of asphalt concrete paving jobs. The temperature of both hot and warm mix asphalt are significantly higher than the surrounding environment. Therefore, the hot mat should be easily identifiable in IR images.

Since one of the objectives of this project was to deliver a low cost solution, therefore after studying the IR cameras available in the market, we chose the FLIR PathFindIR (black and white) as the cheapest camera that met the project's requirements. The main criteria for camera selection were minimum frame rate of 15fps and an industrial design which allows using the camera in harsh environments. The specification for FLIR® PathFindIR (black and white) is listed below:

- Frame Rate: 15fps
- Sensor Type: 320x240 uncooled, 38 micron pitch, 8-14 micron LWIR
- Field of view: 36º H x 27º V
- Video output: Standard NTSC, or PAL
- Hermetically sealed and rated to IP67 for handling harsh environments

Additional equipment used in the experimental setup include:

- 1 x triple suction cup camera mount with adjustments around 3 axis
- 1 x mobile data logger used for video recording, integrated with GPS and accelerometer
- 1 x 7" display screen that displays the real time IR view and system status
- 1 x laptop with 8 Gigs of memory and Intel Core i5 CPU used for data processing

*The GoPro camera was only used for documenting the data collection and was not part of the development rig.

Figure 23Figure 23 describes the setup used on rollers to capture the operator field of view.

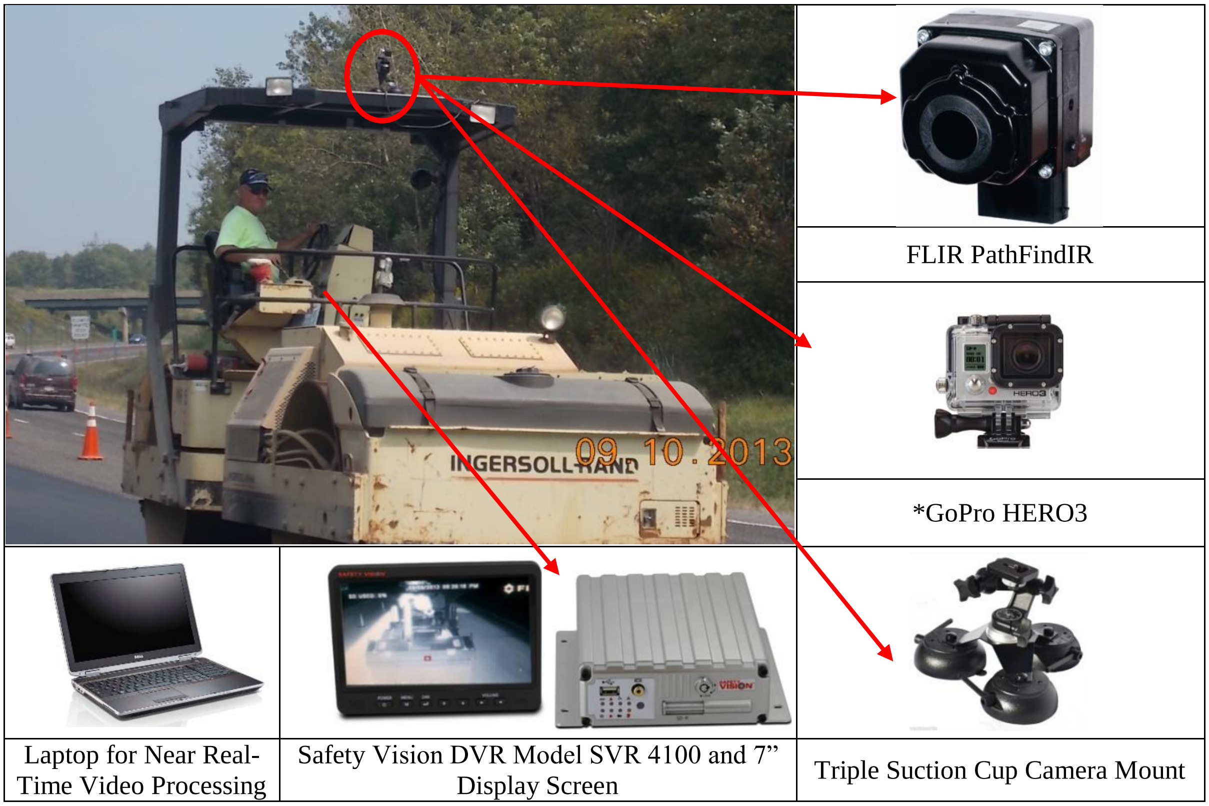

*The GoPro camera was only used for documenting the data collection and was not part of the development rig.

Figure 23 Camera Setup on the Roller

3.2.3. Camera Calibration

In order to make any measurement based on an image, the camera has to be calibrated first. The camera matrix calculated through calibration process, only depends on the camera intrinsic properties. Therefore, once calculated, it can be stored for existing and future applications.

Infrared camera calibration

Originally a checkerboard similar to the typical pattern described in chapter 2, which are used for calibration of optical cameras was used for in this study. To make the pattern visible in LWIR spectrum range, magnet squares were placed on the black squares. The whole pattern was uniformly heated with a heat lamp. As it is shown in Figure 24 Chessboard Heated Pattern-b, the square edges and corners in the image taken by the IR camera are fuzzy (the image is inverted). This is due to the fact that heat disseminates into the air from the heated magnets. Thus, key point extraction for heated chessboard pattern using IR camera is less precise compared to calibration process for optical cameras. Review of the literature in this area indicated that using a heated chessboard pattern alone, and the same calibration algorithm as used for optical cameras will result in projection error greater than 1 [55]. In this study re-projection error for FLIR PathFindIR infra-red camera using a heated chessboard was found to be between 1.2-1.5 after multiple repetitions.

To reduce the re-projection error, innovative methods were found in the literature. In this study, the method recommended by Ellmauthaler et al. [55] was selected to reduce the re-projection error. The methodology includes using a symmetrical circular pattern with an ellipse detection feature, since circles look like ellipses if the calibration pattern is not parallel to the camera plane.

In the calibration module of the software developed in this study, there is an option for ellipse correction which refers to this method. Ellmauthaler et al. also proposed an iterative solution for calibration process. However, based on the limited information available in their paper, reproduction of their program was not possible. Therefore, for calibration of the IR camera, a special symmetric circular pattern, displayed in Figure 25, was developed and the data were processed by Zhang [51] algorithm. Using the circular pattern the re-projection error decreased to approximately 1. The custom design of the pattern include a slot that allowed inserting a heated plate inside the pattern, which makes it visible to the IR camera.

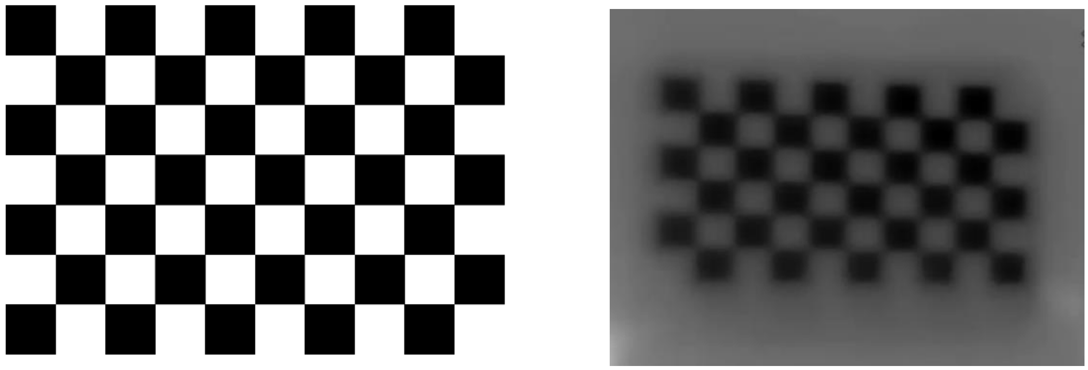

a) Optical Image of a Chessboard Pattern b) IR Image of a Heated Chessboard Pattern

Figure 24 Chessboard Heated Pattern

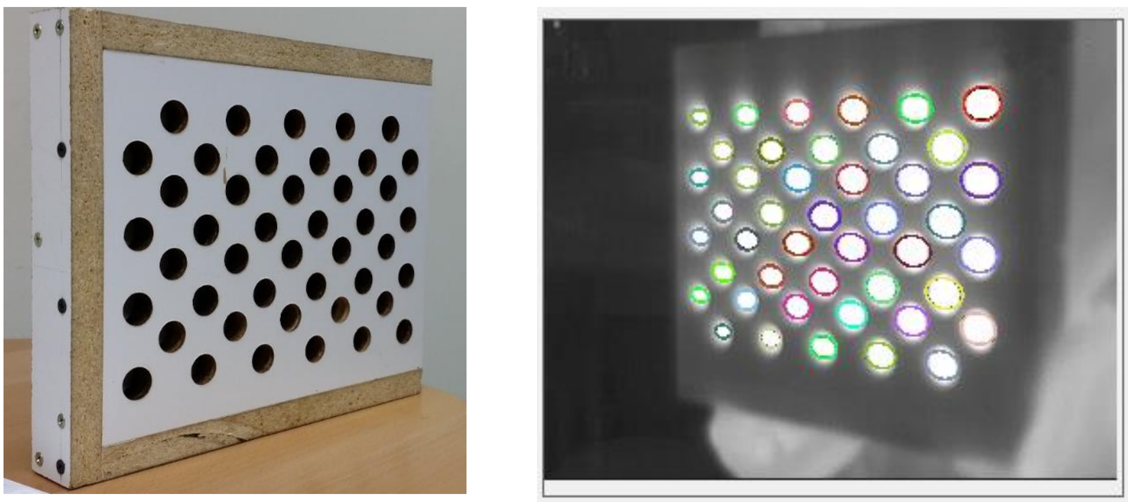

a) Optical Image of a Symmetrical Circular Pattern b) IR Image of a Symmetrical Circular Pattern

Figure 25 Symmetrical Circular Pattern

3.2.4. Visual Odometry

Based on the literature review, a methodology proposed by Campbell et al. [57] for visual odometry was chosen for this study. However, since the Campbell et al. method was developed for using with optical cameras, some modifications were made to improve the results. In the following, the original methodology proposed by Campbell et al. is discussed. Then it is explained why such method could not be as accurate for using in IR vision and finally the modifications that are made to the algorithm will be discussed.

The original visual odometry method by Campbell et al., is based on monocular vision rather than stereo vision which helps developing a simpler, and more cost effective device but is restricted to planar surfaces. Surface planarity is the primary assumption of the solution. The assumption of planer surface is valid for paving projects to a great extent. The method includes the following steps:

1. Mapping Camera Coordinates to the Ground Plane

In this step, the required transformation between the camera plane/image coordinates (u,v) of a tracked feature and its corresponding point (x,y) on the ground plane is calculated. The origin of the image coordinate system is placed on the upper left corner of the image. The schematic of the system is presented in Figure 26. “H” is a user input and denotes the height of the camera from the ground, D is the distance from the roller to the intersection of the principal ray with the ground plane. Thus, the camera tilt, “α” can be calculated from Equation 16:

$$\alpha = \tan^{-1}\left(\frac{H}{D}\right) \qquad \text{Equation 16}$$

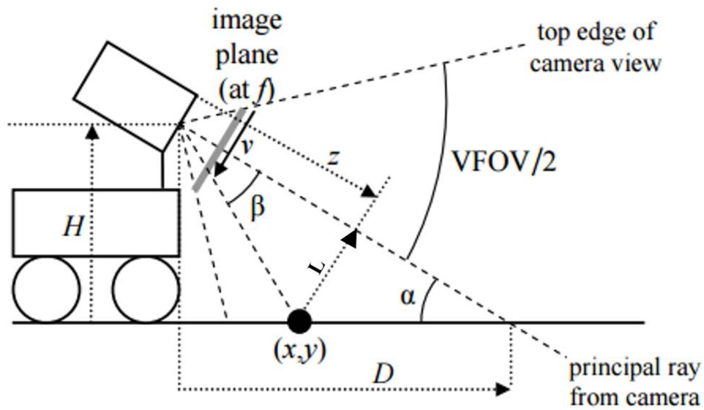

Figure 26 Mapping Camera Coordinates to the Ground Plane [57]

From trigonometry, one can show:

$$\frac{v - \frac{V}{2}}{L} = \frac{f}{z}$$

Where $L = z\tan(\beta)$ and $f = \frac{V}{2\tan(\frac{VFOV}{2})}$

The vertical angle between focal point and the observed point is recovered from Equation 17 [57][1]:

$$\tan(\beta) = \frac{(2\vartheta - V)}{V}\tan\left(\frac{VFOV}{2}\right) \qquad \text{Equation 17}$$

Where

[1] The original equation in [55] is: $\tan(\beta) = (2\vartheta - V)\tan\left(\frac{VFOV}{2}\right)$. After verifying the math, it was found that $\tan(\beta) = \frac{(2\vartheta - V)}{V}\tan\left(\frac{VFOV}{2}\right)$

"V" is the image height,

"z" is defined as the depth of the observed point from the camera ,

"*f" is the focal distance'*

And "VFOV" is the vertical field of view of the camera

Once α and β are known the distance from the roller is given by Equation 18:

$$y = \frac{H}{\tan(\alpha + \beta)} \qquad \text{Equation 18}$$

"z" can be recovered from Equation 19:

$$z = \frac{Hcos(\beta)}{\sin(\alpha + \beta)} \qquad \text{Equation 19}$$

2. Estimating Roller Rotation and Translation

Over a short interval, the roller's movement on the ground plane can be decomposed into a change in heading (rotation about a vertical axis) and a displacement (translation). To recover the roller's heading and translation from a series of successive images, the concept of optical flow must be introduced first. Optical flow is the pattern or 2D projection of the physical movement of objects, surfaces, and edges in a visual scene caused by the relative motion between an observer (an eye or a camera) and the scene. Optical flow concept was developed based on the Lucas and Kanande [41] work on image registration which was discussed in chapter 2. The assumption is that the appearance of the image i.e. brightness constancy remains the same over small regions in the image. Thus:

$$I(x+u, y+v, t+1) = I(x, y, t) \qquad \text{Equation 20}$$

Where:

I is the image density

t is the time

(u,v) is the displacement vector

(x,y) is the feature coordinate

From constancy in brightness, we can drive Equation 21:

$$\left.\frac{\partial I}{\partial x}\right|_{t}\left(\frac{\partial x}{\partial t}\right)+\left.\frac{\partial I}{\partial t}\right|_{x(t)} = 0 \qquad \text{Equation 21}$$

If we denote $I_x = \frac{\partial I}{\partial x}$, $I_t = \frac{\partial I}{\partial t}$

$$\Rightarrow v = \frac{I_t}{I_x} \qquad \text{Equation 22}$$

Where v describes the one dimensional velocity vector, as illustrated in Figure 27.

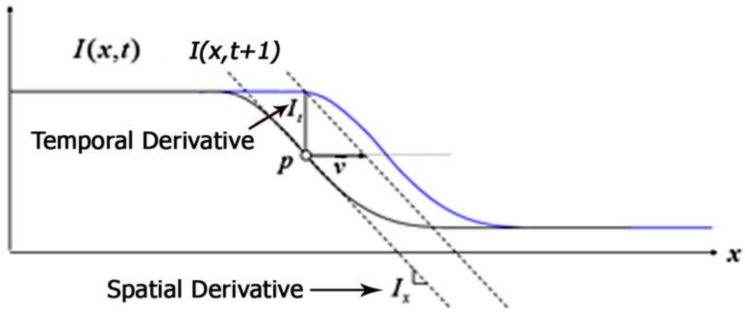

Figure 27 1D Optical Flow Estimation

For 2D tracking we have:

$$\left.\frac{\partial I}{\partial x}\right|_t \left(\frac{\partial x}{\partial t}\right) + \left.\frac{\partial I}{\partial y}\right|_t \left(\frac{\partial y}{\partial t}\right) + \left.\frac{\partial I}{\partial t}\right|_{x(t)} = 0$$ Equation 23

$$\left.\frac{\partial I}{\partial x}\right|_t u + \left.\frac{\partial I}{\partial y}\right|_t v + \left.\frac{\partial I}{\partial t}\right|_{x(t)} = 0$$ Equation 24

$$I_x u + I_y v + I_t = 0$$ Equation 25

$$\nabla I^T u = -I_t$$ Equation 26

Where $u = \begin{bmatrix} u \\ v \end{bmatrix}, \nabla I = \begin{bmatrix} I_x \\ I_y \end{bmatrix}$

A sequence of ordered images could be used to estimate motion as either instantaneous image velocities or discrete image displacements. An example of optical flow representation is presented in Figure 28. This image is simply provided as an example of changes in the optical flow based on the near features and distant features. As it can be seen in the image, distant features from the camera exhibit very small amounts of parallax-induced optical flow.

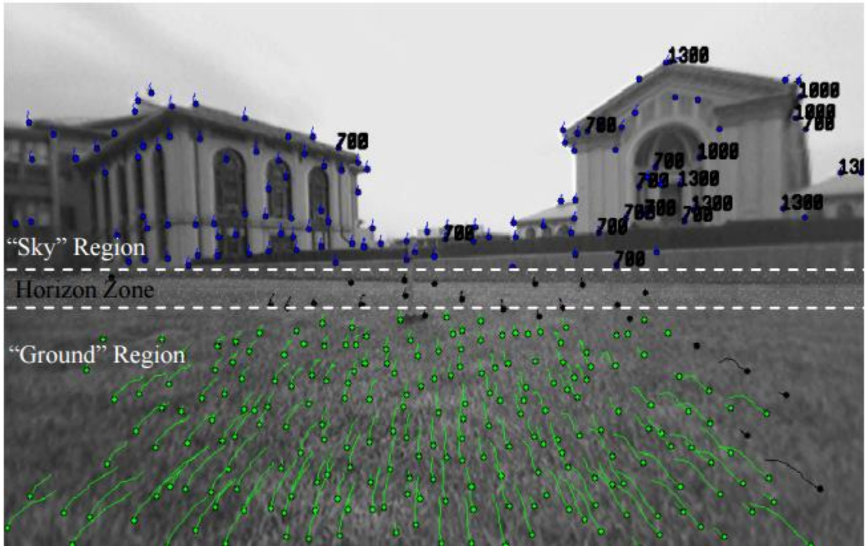

Figure 28 Optical Flow Estimation [57]

Generally, the optical flow vectors below the horizon corresponds to the points that are close to the roller and are good for translation estimation. The vectors above the horizon mostly refers to the distant features that are not suitable for translation estimation but still could be used for rotation estimation. The area close to the horizon must be excluded from path estimation, as it can cause error in the calculation. Therefore, each image is divided into three regions denoted as sky (above the horizon), dead zone (around the horizon), and ground (below the horizon). Sky and ground regions are used for rotation and translation calculations, respectively. Although roller rotation affects the optical flow of both near and distant features with the same change in heading, but since the distant features are relatively insensitive to the optical flow induced by translation, thus distant features are selected for rotation analysis. Figure 29 illustrates the translation effect on heading measurement. If we assume that the two features in Figure 29 are fixed and the roller is following a straight path without any change in the heading, the measure of heading still will be affected by the translation (a'≠a and b'≠b). However, the effect is less significant for measurements based on distant features (|b-b'|<<|a-a'|).

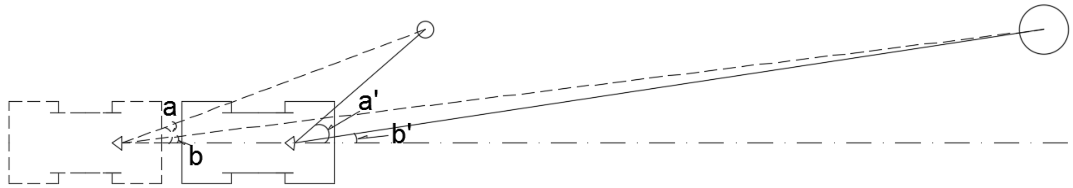

Figure 29 Effect of translation on heading measurement

To justify why it is safe to ignore the translation effect on the change of heading measured from distant objects, the magnitude of translation between two frames must be considered. Based on the recommended rolling speeds provided in Table 2 [58], the maximum rolling speed is about 12 km/hr or 3.3 m/s (~11 ft/s). The cameras used in this study can capture 15 frames per second. It means the maximum expected translation between two subsequent frames is about 22 cm (~9 in). Therefore, for such a small translation per frame, we can ignore the translation effect on the optical flow of distant features.

Table 2 Recommended rolling speeds

Speed (km/hr)	Task
4-6	Breakdown compaction (static rolling with tandem rollers)
3-5	Intermediate compaction (static rolling with tandem rollers)
3-5	Intermediate compaction (Vibration)
4-12	Intermediate compaction (Pneumatic tired roller)
6-8	Finish rolling (static rolling with tandem rollers)

To measure the heading, flow vectors in the sky region are back projected into a vertical cylindrical coordinate system, centered on the camera. Roller displacement between two consecutive frames can be decomposed into a change in heading (rotation about a vertical axis) and a displacement (translation). The heading is recovered from Equation 27.

$$Heading = \tan^{-1}(\frac{u - C_u}{f_y}) \qquad \text{Equation 27}$$

Where

C(u,υ) is the center of image in image coordinate system

“u” is the lateral coordinate of the detected feature

f_y is the focal point coordinate along the y access of the camera

The Issue for Implementation in IR Vision

Due to the thermal uniformity of the background (mostly the area designated as the sky region) in IR vision, especially during the night, less features could be detected for analysis of roller’s heading. To compensate for the loss of features in the sky region, which only affects the heading analysis, the following modification was done to the original method by Campbell et al. developed for optical cameras.

Modification for IR Implementation

To increase the system reliability, the possibility of adding other features for rotation analysis were studied. Since, the mat width is generally fixed and the hot edges are distinctive features in

IR images, thus they could be selected for rotation analysis. As illustrated in Figure 30, due to the perspective effect the parallel edges of the mat are sloped in the images. The slopes should be symmetric only if the camera on the roller is parallel to the edges. In other words, if the image plane is not perpendicular to the road edges, the slopes will appear unsymmetrical in the image. The slope(s) of the edges is/are independent of roller lateral location on the map, for illustration compare state 1 vs 2 in Figure 30. The slope(s) of the edges will not change as long as the roller is following a straight path. As illustrated in state 3 of Figure 30, once the roller's heading changes, the slope(s) of the edges will change too. The change in roller's heading, described by α is the difference between the angles of the edge slopes in two successive images denoted by β and γ. Either of the edges could be used for rotation analysis, however depending on the roller's lateral location, camera's shooting angle or field of view, there might be cases where only one edge is visible in the image.

The issue with using edge slope is that it could be influenced by road curvature. However, the curve affects the slope when it is observed in the distance while the edges near to the roller the edges are straight. Therefore the edge selection will be only performed in the ground region of the image.

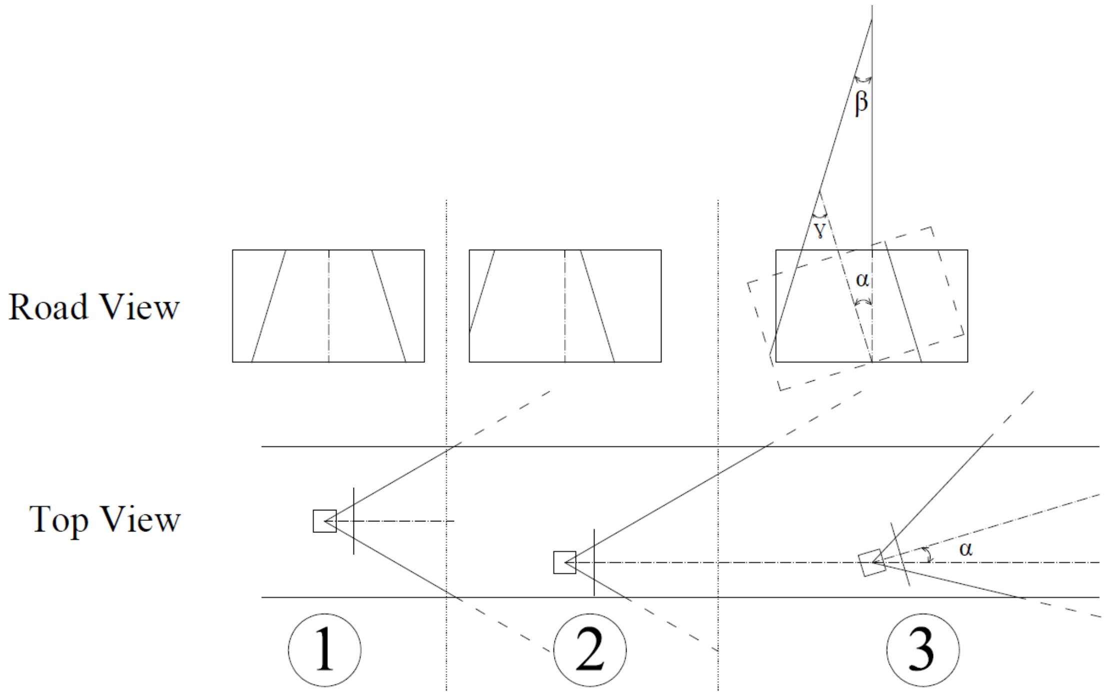

Figure 30 Illustration of geometric approach to estimate the change in roller's heading

Canny edge detector discussed in chapter two was used to detect the mat edges. Canny returns a series of points along the mat edges. The next step is to fit a line through the edge points that is as close as possible to the mat edges. In each image captured by the IR camera placed on the roller, there could be as many as two edges visible. As discussed in chapter 2, there are different techniques available to construct a straight line based on the points from edge detection. Hough transform was selected in this research because it performs segmentation and line detection simultaneously. Therefore, it is possible to detect both edges at the same time. There are two functions in OpenCV that implement Hough transformation, a simple Hough transform and a probabilistic Hough transform. The first function outputs an array of (θ, r_θ) which includes all detected lines in polar coordinates. The probabilistic function provides a more efficient implementation of Hough transform by allowing the user to input the minimum number of points required to form a line, the line angle, thickness and the maximum gap allowed between two points that could be considered on the same line. The function outputs an array that includes the beginning and the end of each line detected. The probabilistic Hough transform was used in this study, because it allows filtering out small lines due to roller marks, the slopes close to horizontal line and joining shorter edge segments to construct longer lines along the edge. Using the beginning and end point of each detected line by Hough transform, the slope of each line was calculated. Due to the perspective effect, the slope of the lines fitted to the right edge will be positive and the slope of the lines fitted to the left edge will be negative. The measured slopes will be grouped based on their sign and the median of each group will be assigned to the respective edge as the representative slope. The angle constructed between the extension of each edge of the mat and the centerline of the image displayed in Figure 30 will be recovered from Equation 28 and Equation 29.

$$\beta = \tan^{-1}\left(\frac{m_{edge} - m_{centerline}}{1 + m_{edge}m_{centerline}}\right) = \tan^{-1}(m_{edge}) \qquad \text{Equation 28}$$

$$\gamma = \tan^{-1}\left(\frac{m'_{edge} - m'_{centerline}}{1 + m'_{edge}m'_{centerline}}\right) = \tan^{-1}(m'_{edge}) \qquad \text{Equation 29}$$

Where m_{edge} and m'_{edge} correspond to i^{th} and $i\text{-}1^{th}$ frames respectively.

$$\alpha = \gamma - \beta \qquad \text{Equation 30}$$

Homography Matrix Calculation

To measure the translation, first the rotational flow field must be subtracted based on the estimated heading. Then to calculate the pure translation, the flow vectors must be back-projected on to the ground plane. For such a transformation that provides the top-down (bird's eye) view and is essential to remove the perspective effect, a homography matrix has to be calculated.

Homography is a 3 by 3 matrix that relates the pixel coordinates between two images. Once a homography matrix is applied to an image, it will remap every pixel in the image to create a new image from the original image, see Figure 31 for illustration. To estimate a homography matrix, one may start with knowing that X2 ~ HX1, where X1, X2 are unique coordinates in the original image and transformed image, respectively and H is the homography matrix. Thus in homogenous coordinates:

$$\begin{bmatrix} x_2 \\ y_2 \\ z_2 \end{bmatrix} = \begin{bmatrix} H_{11} & H_{12} & H_{13} \\ H_{21} & H_{22} & H_{23} \\ H_{31} & H_{32} & H_{33} \end{bmatrix} \begin{bmatrix} x_1 \\ y_1 \\ z_1 \end{bmatrix} \Leftrightarrow X_2 = HX_1 \qquad \text{Equation 31}$$

In in-homogenous coordinates ($x_2' = \frac{x_2}{z_2}$ and $y_2' = \frac{y_2}{z_2}$),

$$x_2' = \frac{H_{11}x_1 + H_{12}y_1 + H_{13}z_1}{H_{31}x_1 + H_{32}y_1 + H_{33}z_1} \qquad \text{Equation 32}$$

$$y_2' = \frac{H_{21}x_1 + H_{22}y_1 + H_{23}z_1}{H_{31}x_1 + H_{32}y_1 + H_{33}z_1} \qquad \text{Equation 33}$$

Without loss of generality, set $z_1 = 1$ and rearrange:

$$x_2' \left(H_{31}x_1 + H_{32}y_1 + H_{33}\right) = H_{11}x_1 + H_{12}y_1 + H_{13} \qquad \text{Equation 34}$$

$$y_2' \left(H_{31}x_1 + H_{32}y_1 + H_{33}\right) = H_{21}x_1 + H_{22}y_1 + H_{23} \qquad \text{Equation 35}$$

Although these inhomogeneous equations involve the coordinates nonlinearly, the coefficients of *H* appear linearly. Thus, Equation 34 and Equation 35 were rewritten as:

$$a_x^T h = 0 \qquad \text{Equation 36}$$

$$a_y^T h = 0 \qquad \text{Equation 37}$$

Where:

$h = (H_{11}, H_{12}, H_{13}, H_{21}, H_{22}, H_{23}, H_{31}, H_{32}, H_{33})^T$

$a_x = (-x_1, -y_1, -1, 0, 0, 0, x_2'x_1, x_2'y_1, x_2')^T$

$a_y = (0, 0, 0, -x_1, -y_1, -1, y_2'x_1, y_2'y_1, y_2')^T$

Using a set of corresponding points, the following linear system of equation are solved:

$$Ah = 0 \qquad \text{Equation 38}$$

Where

$$A = \begin{pmatrix} a_{x1}^T \\ a_{y1}^T \\ \cdot \\ \vdots \\ a_{xN}^T \\ a_{yN}^T \end{pmatrix}$$

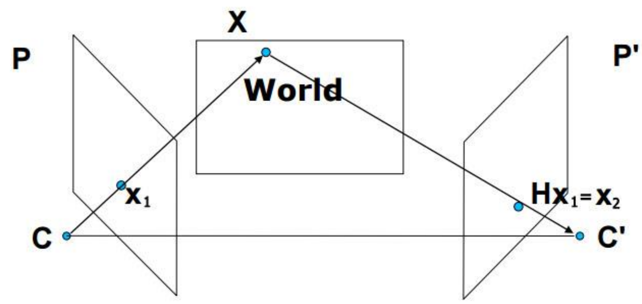

Figure 31 Plane Transfer Homography

3.2.5. Estimating Global Motion

The incremental deviations in the roller pose are linked frame-by-frame to derive the global estimate of the roller's position.

3.2.6. Software Development

Once a sequence of images is available from the camera, it is time to process the images and produce as much as helpful information as possible in near real-time. There are a variety different platforms and software available for image processing. The most common platforms include MATLAB and Open source computer vision library (OpenCV), the latter is a C++ library. OpenCV is an open source library for both computer vision and machine learning. It was built to facilitate a common infrastructure for CV applications and it is free for both academic and commercial use. In addition, OpenCV design was based on computational efficiency with a strong emphasis on real-time applications. Perhaps the most useful part of OpenCV is its architecture and memory management. It provides users with a framework in which one can work with images and videos using OpenCV's algorithms or user developed algorithms, without worrying about allocating and de-allocating memory for images. OpenCV has C++, C, Python, Java and MATLAB interfaces and supports Windows, Linux, Android and Macintosh operating systems [59]. Based on the project requirements and the advantage of being open source, OpenCV was chosen for software development in this study.

A user friendly interface can always promote software application, therefore one of the objectives of the software development in this project was to develop a friendly graphical user interface (GUI). C# is one of the programming languages that provide developers with the tools required for developing windows based GUIs. Fortunately, there is a C# wrapper for OpenCV library which is called EmguCV. Using EmguCV, one can use the majority of OpenCV functions in C# as well as benefiting from C# GUI development toolbox. Eventually, C# and EmguCV were used for software development.

3.2.7. Software Demonstration

The software has a modular design. The startup page, shown in Figure 32, allows the user to start choosing between calibrating the camera, roller tracking and viewing logged projects and help.

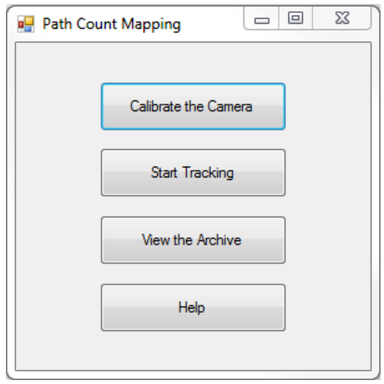

Figure 32 Startup Page

Camera Calibration Form

Camera calibration is necessary whenever a new camera is being used. Once the camera parameters are retrieved, the parameters will be saved in a text file under

"...Project Directory\RollerPath\CalibrationFiles\Calibration_Output.txt"

The camera calibration module displayed in Figure 33, allows calibration of both regular and infrared cameras. The infrared calibration is done only for the purpose of finding the camera matrix. This module, allow calibration using checkerboard, symmetric and asymmetric circular patterns for calibration of IIR camera. However, using a heated checkerboard pattern generally result in re-projection errors larger than one.

The functionality and the purposes of buttons and options available in the camera calibration module are described in the following:

Start: The start button allows access to the camera video stream and displays the video in the top-left box. If histogram equalization is checked, the intensity of the input stream is adjusted to enhance contrast before being displayed or grabbed for processing. The user can adjust the equalization level and visually examine the results. If the “Infra-Red Camera” box is checked, the input image will be inverted for better visualization of heat sources.

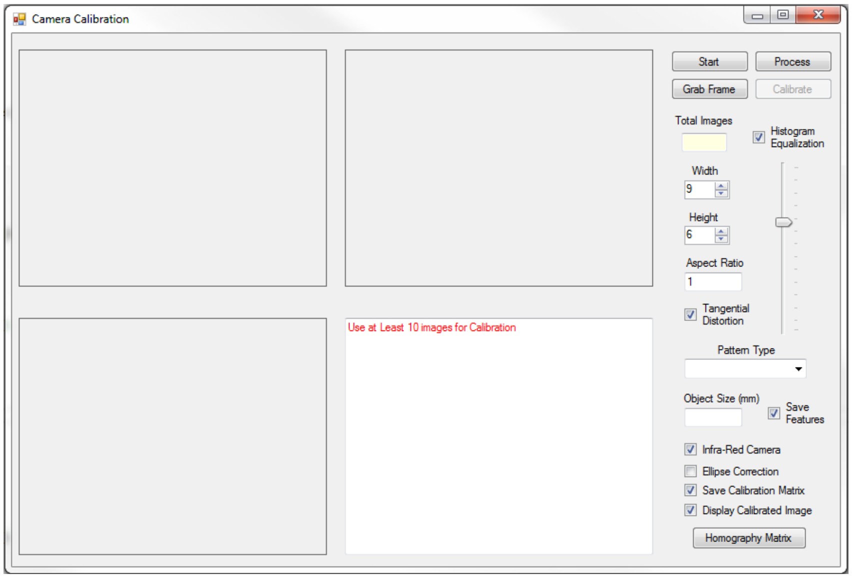

Figure 33 Camera Calibration Module

Grab Frame: Once the user finds the appropriate view of the calibrating pattern in the top-left window, pressing the “Grab Frame” will pick the frame for calibration.

Process: The process button collects all the user input parameters, including: the number of images used for calibration, the pattern size (width, height), aspect ratio, pattern type (Chessboard, Circular, and Asymmetrical Circular), and the size of features in the pattern.

Calibrate: The calibrate button uses the calibration algorithm available in OpenCV for calibration. Once the calibration process is done, calibration parameters are displayed in the text box. The calibrated images are also be displayed for visual examination of the results. If the re-projection error is more than 1.0, the program will recommend recalibration using a new set of image.

Homography Transformation Form

To calculate roller translation based on images, the perspective effect must be corrected. An image is only free of perspective, if taken perpendicular to the plane containing the object. In this case, top-down (bird's eye) view of the paving lane is required for processing. To calculate the birds eye view, at least four pairs of corresponding points are required. For this project, the camera is placed on the top a roller and faced toward the paving lane. Due to the perspective effect, the width of paving lane decreases with the distance from the roller, however, in reality the lane edges are parallel. This feature was used for back calculation of the homography matrix. As described in

Figure 34, the user can grab an image from a camera/recorded video or load a saved image. Then, user has to pick four points (p_1, p_2, p_3, p_4) such that they create a rectangle along the edges of the paving lane.

The markers on the side of the display window can help easier selection of the points. The actual coordinates of the selected points relative to the camera center are calculated from user inputs including paving width, roller distance to the rectangle, and rectangle height. A visual guide for users to enter the relative geometry of the selected points is provided at the bottom of the form.

Homography: The homography button calculates the homograhy matrix from comparing the coordinates of the selected points with their actual coordinates relative to the camera center. Since the actual coordinates are not affected by perspective, the homography matrix is calculated such that will remove the perspective from the image. Once the calculation process is over, the software displays the top down view image for visual inspection of the results and the calculated matrix will be saved under:

"…Project Directory\RollerPath\CalibrationFiles\homo_calc.txt"

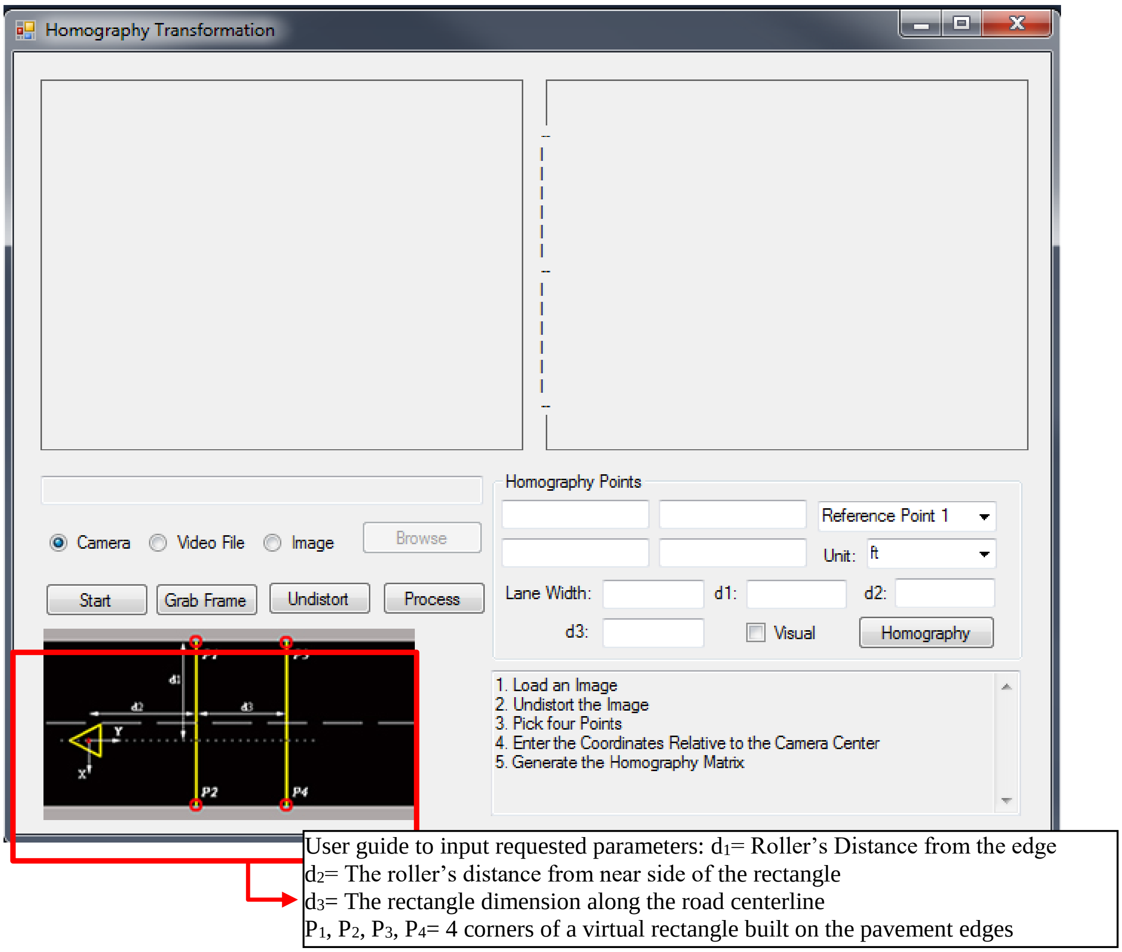

Figure 34 Estimation of Homography Matrix

Roller Tracking Form

The "Roller Tracking" module displayed in Figure 35 is where the feature detection occurs. This window also provide general information such as frame rate, number of features detected, distance traveled and also allows the user to choose the unit system. Every frame from the camera is corrected by the calibration matrix calculated using the camera calibration module, before being displayed in this module. The user has to define the horizon lines to separate the sky and ground regions. These are the horizontal red lines in Figure 35. This is done at the beginning of each compaction job and because of the planar surface assumption the horizon line is not expected to change throughout the project.

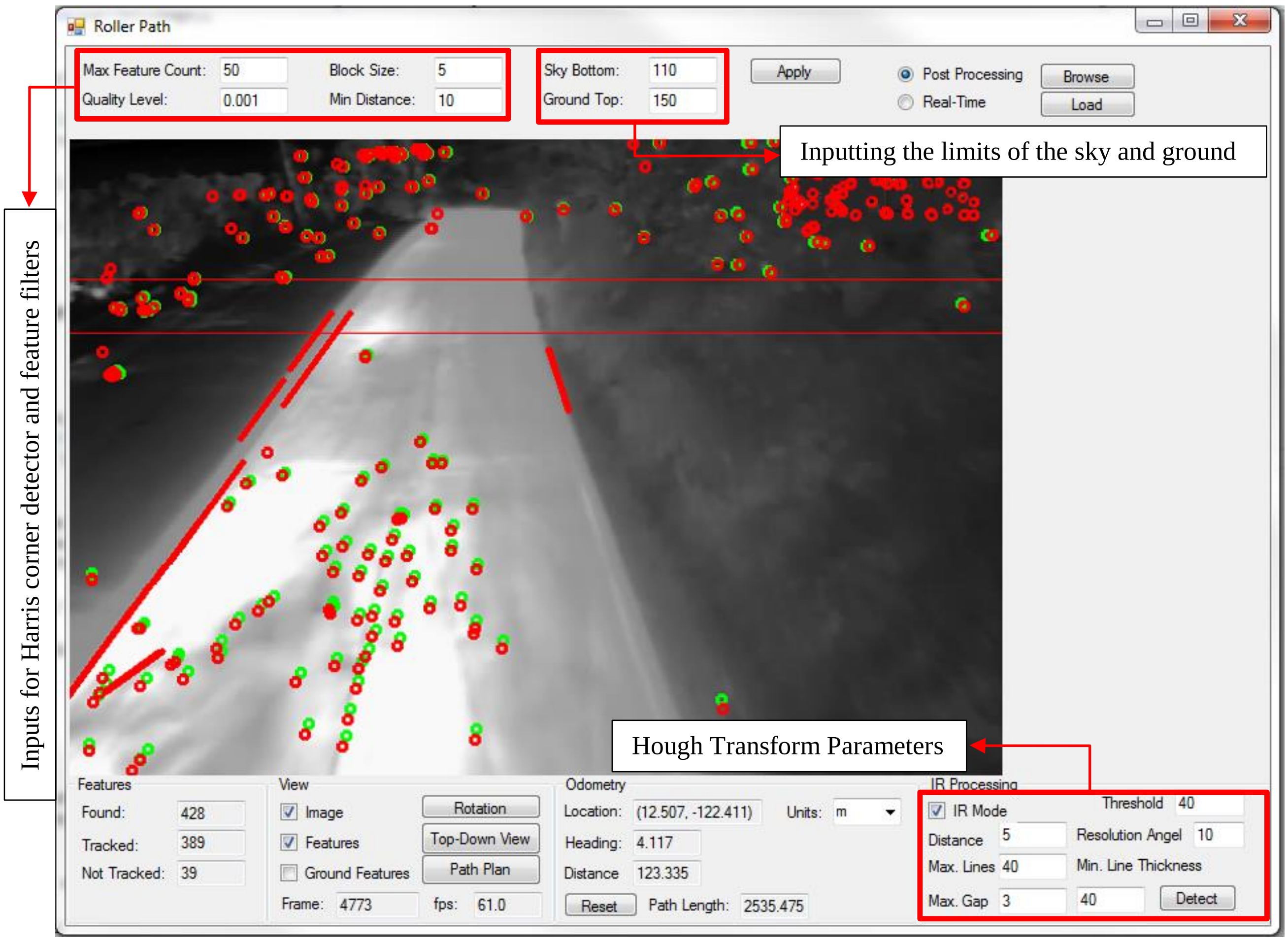

Figure 35 Roller Tracking Module

The program also uses a *"Harris"* corner detector for feature selection. The red dots in Figure 35 are the features originally detected by the Harris corner algorithm. However, in reality not all of the detected features are fixed. Tracking based on moving features introduces error in the calculation. Therefore, to assure that the detected features are reliable for tracking, historical information on the feature behavior are required. The red features are tracked in 5 consecutive frames after detection. If a feature is stable for 3 frames, its color will turn into yellow and finally will change to green if its historical record reaches 5 frame. Only green features are qualified for roller path calculation. The user has to pick a block/window size for Harris corner detection algorithm. This parameter usually depends on the image resolution, computation capacity, type of processing (real-time vs post processing), and image scene uniformity. Therefore, it could be different from job to job and if the hardware is changed. Other parameters such "Quality Level", and "Min Distance" will help to filter out the outliers. The "Max Feature Count" sets a limit for the maximum number of features detected in a frame and avoids overwhelming the system processing capacity. In chapter 4, three sets of input parameters are used to evaluate the system performance.

Once reliable features are available on the ground, both roller's translation and heading can be determined. The heading change, calculated based on edge detection is also added to the pool of headings measured from sky features. The median of the pool will be selected for heading analysis. To estimate the roller's translation, the perspective effect has to be removed from the image. Therefore a perpendicular/top-down view of the surface is required. The homography matrix calculated using the homography module is used to estimate the top-down view as displayed in Figure 36. The translation calculation in the top-down view is only performed on the ground portion of the frame. The features in the sky portion and edge slopes in the ground portion are analyzed for *"Heading" measurement*. The median of the headings calculated for each stabilized feature is used as the true angle of rotation for motion estimation.

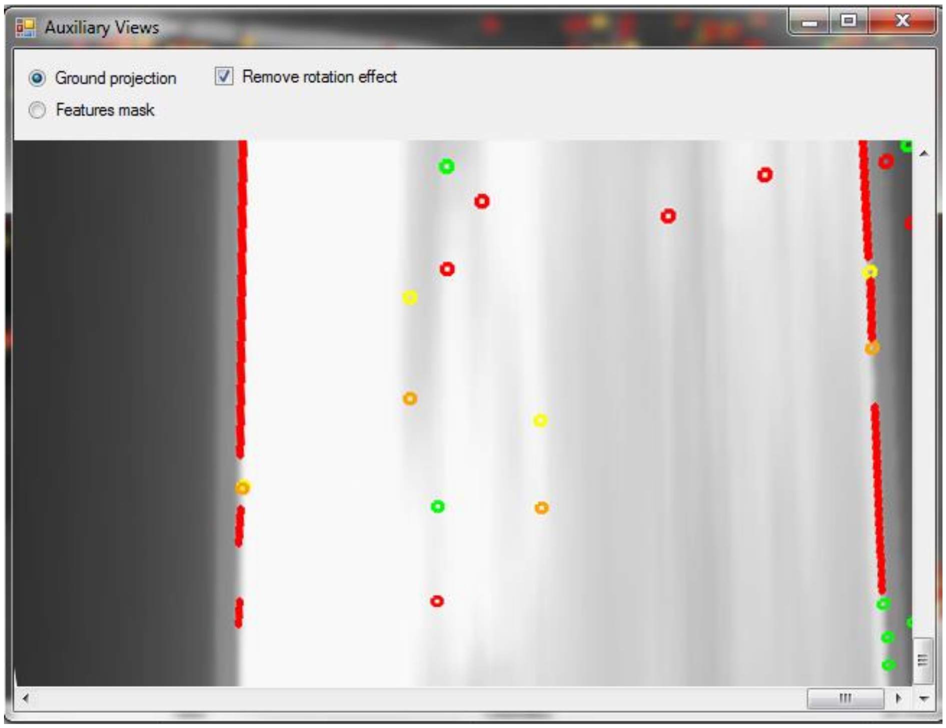

Figure 36 Top-Down View

Roller Pass Tracking View

The roller track points are periodically repopulated and the tracking map displayed in Figure 37 is updated. Before start rolling, operator has to input the roller width and the required number of passes to accomplish the compaction in the map view window. As the roller moves over the surface the overlaps of the roller width will be painted with a new color. The color is selected from the RGB color system from red to green. Color selection is a function of number of accomplished passes to the total number of required passes. The first pass is always displayed in red and once it turns green the required number of passes is achieved. The white regions refer to those areas where roller has not been operated. The produced color coded map assists the roller operator to uniformly compact the entire surface with the required number of passes.

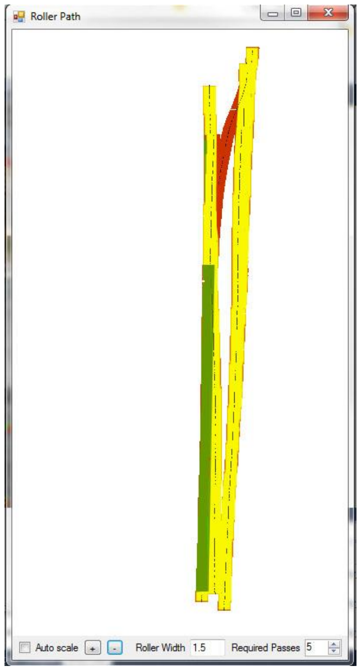

Figure 37 Roller Path Tracking (Color is a function of number of accomplished passes to the required passes, ranging from red to green)

Chapter 4: **RESULTS**

4.1. INTRODUCTION

The methodology and the software developed in this study was used in the field for performance evaluation. In the following, the methodology performance using the different types of cameras are discussed.

4.2. PERFORMANCE EVALUATION

Two evaluate the performance of a tracking system based on visual odometry generally two modes are considered:

- Open loop: passive observation of the roller's motion
- Closed loop: integrated with the roller's machine control sensors such as the odometer

Closed-loop evaluation is more beneficial and commonly used practice, but open loop testing is also important and informative for evaluating a tracking system based on visual odometry. This is because, when conducting a closed loop test, in certain modes (e.g., when moving straight along one axis), a variety of test parameters may yield satisfactory performance. By contrast, open loop evaluation spotlights bias errors in translational and angular motion estimation that that contribute to cumulative error.

The system evaluation provided in this chapter is based on post processing of IR videos collected from 4 different job sites listed in Table 3. The table also include information about roadway system and whether the data has been collected during the day or night. These information is important for system performance evaluation, as in IR vision, on freeways due to the wider right of way, there are less features in the background compared to county roads, for illustration compare Figure 38-a vs Figure 38-b. Moreover, since the different materials in nature have different capacity to reflect/absorb heat, thus in IR vision, there are more features in the background during the day compared to night, when temperature is more uniform, for illustration compare Figure 38-a and Figure 38-b vs Figure 38-c.

Table 3 Summary of the test sites used system evaluation

No.	Test Location	System	Test Date	Day/Night
1	I-79S close to Shinnston, WV	Freeway	09/05/2013	Day
2	I-68E MP 24	Freeway	09/10/2013	Day
3	Saltwell Rd., Shinnston, WV	County Rd.	10/08/2013	Day
4	US 50W, Outside Clarksburg, WV	Freeway	10/14/2013	Night

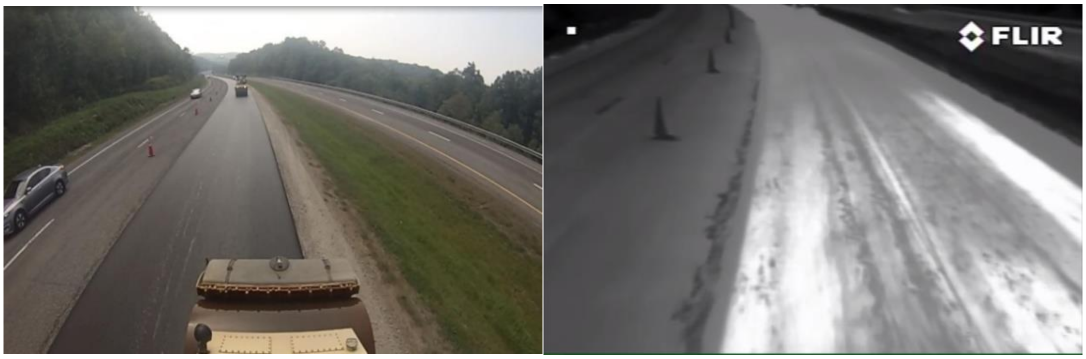

a) I-68E MP 24

b) Saltwell Rd., Shinnston, WV

c) US 50W, Outside Clarksburg, WV

Figure 38 Compares IR view of different landscapes during day and night

Since the developed system acts as an independent unit that only relies on the roller for power supply, no data from the roller control unit including the odometer was integrated in data collection. Therefore, the evaluations provided here are classified as open loop. The following three types of position estimation error were studied:

a) Incremental translational error for each roller pass:

   The length of each path was estimated from GPS coordinates or local mile posts. The distance traveled during each pass was measured by the device and then divided by the reference length to estimate the error.

b) Incremental rotational error:

   Since no independent device was available to record roller's rotations, this test was defined as a Pass/Fail criteria, determining the number of system successes/failures to detect roller's rotations.

c) Cumulative translational error:

   The cumulative distance traveled by the roller to complete a coverage was measured by the system and the results were divided by the reference length to estimate the system error.

In addition system performance during day vs night and freeway vs county road were evaluated.

4.3. TEST SCHEME

Since the system inputs for Harris corner detection, Canny, and Hough transform algorithms affect the system performance, three sets of system inputs based on low, medium and high level of computation efforts were defined and are described in the following:

1. Level of computation effort: Low

Harris Corner Parameters:

Max Feature Count: 50
Block size: 20
Quality Level: 0.1

Hough Transform:

Distance: 10
Max Line Detected: 10
Max Gap: 40
Min Line Thickness: 5

2. Level of computation effort: Medium

Harris Corner Parameters:

Max Feature Count: 100
Block size: 10
Quality Level: 0.01

Hough Transform:

Distance: 5
Max Line Detected: 20
Max Gap: 40
Min Line Thickness: 10

3. Level of computation effort: High

Harris Corner Parameters:

Max Feature Count: 200
Block size: 5
Quality Level: 0.001

Hough Transform:

Distance: 1
Max Line Detected: 40
Max Gap: 40
Min Line Thickness: 15

4.4. TEST RESULTS

The test scheme was used to conduct post processing on the data collected from the four sites described in Table 3. The results are provided in Table 4:

Table 4 Post Processing results

Site No.	Test Scheme	Incremental Translation				Incremental rotation		Cumulative translational		
		Ref. Dist(m)	Average System Measurement (m)	COV	Error	Success (per coverage)	Failure (per coverage)	Ref. Distance(m)	Average System Measurement (m)	Est. Error
1	1	63	Complete Failure	---	---	Complete Failure	---	631.5	Complete Failure	---
	2		56.57	0.07	11%	14	0		561.63	11.2%
	3		53.16	0.02	1.2%	14	0		644.48	2%
2	1	88	Complete Failure	---	---	Complete Failure	---	968	Complete Failure	---
	2		80.17	0.05	9.7%	16	0		1070.5	10.6%
	3		84.19	0.04	4.4%	16	0		1024.22	5.7%
3	1	140	Complete Failure	---	---	Complete Failure	---	699	Complete Failure	---
	2		148.4	0.08	5.9%	13	0		733.42	7.8%
	3		144.86	0.06	5.6%	13	0		647.87	7.3%
4	1	198	Complete Failure	---	---	Complete Failure	---	1779	Complete Failure	---
	2		187.45	0.08	5.2%	11	0		1904.67	7%
	3		191.76	0.06	3.0%	11	0		1877.3	5.4%

Studying the results presented in Table 4, indicates that the system performance highly depends on the input settings. Generally by decreasing the block size which explores the image for features, increasing the maximum number of allowable features and reducing the quality criteria for feature detection the overall error decreases significantly. This effect is less significant for site number 3, which had more features in the background.

Based on Table 4, in short distances the error is almost less than 5% while as expected, the cumulative error is generally higher. As mentioned earlier, the reference measurements were made based on the GPS coordinates or roadway mileposts which may contribute to the calculated error. Therefore, the coefficient of variation was calculated to evaluate the system consistency and repeatability. The low COV values are very promising, and perhaps a more extensive field evaluation may reveal less error.

Chapter 5: **DISCUSSION**

As mentioned in the Chapter 3, the methodology used in this study is based on the planarity assumption. During the development and tests, it was found that the system results achieve higher reliability on freeways compared to some local roads. As the design specification for freeways require a lower longitudinal slope compared to local roads.

System performance also highly depends on angle of shooting, vibration, calibration and user input parameters for Harris corner detection. The significance of each of these parameters are briefly discussed in the following.

5.1. SURFACE SLOPE

Surface planarity is the primary assumption of the solution proposed in this study. Figure 39 illustrates that if the surface plane changes without updating the homography matrix, then the top-down view will not return the true translation.

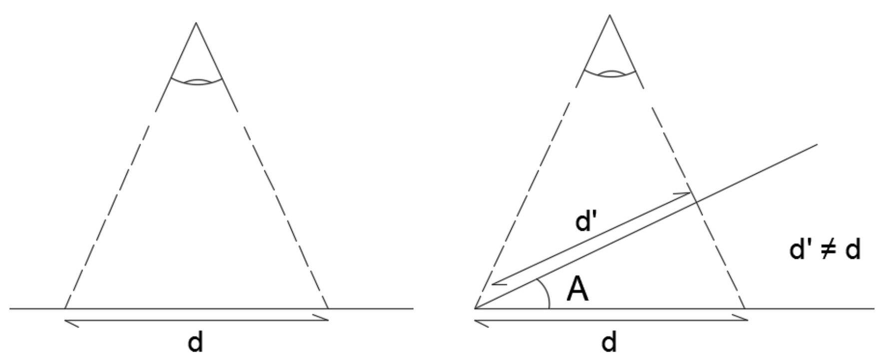

Figure 39 Planarity Assumption

5.2. ANGLE OF SHOOTING

During the tests, it was found that angle of shooting can have significant effect on the accuracy of tracking results. Camera must be mounted at an angle that increases the chance to detect both edges while the roller body should entirely stays out of the camera field of view. A general role of thumb is that to select the shooting angle such that the horizon line would be placed about one third (1/3) of the image height from the top of the image.

5.3. VIBRATION

Vibration can drastically reduce the quality of the results, since vibration is captured as motion between frames. Therefore, using anti-vibration mounts are recommended but were not tested in this study.

5.4. CALIBRATION

Camera matrix is the major output of the calibration process. All the heading calculations are based on the image center and focal point that is recovered from the calibration process. Thus, calibration make a significant contribution to the result accuracy and projection errors greater than 1 are not recommended.

5.5. USER INPUT PARAMETERS

Depending on the image distribution, it was found that the size of window/block and quality level for Harris corner detector, Canny threshold, and Hough transform parameters including: the distance and max gap between lines can significantly affect the result. For images with more uniform distribution, larger window/block sizes can improve the results.

Chapter 6: **CONCLUSIONS AND RECOMMENDATIONS**

6.1. CONCLUSIONS

A new device and the accompanying software was developed in this study. The technology used for roller pass mapping is radically different from the common practice and in some ways is superior. Upon proper training, the information provided by this technology to the operator can improve the construction quality and durability of asphalt concrete pavements. Highway agencies and contractors both will benefit from this device through from omitting or reducing the labor effort for quality control. In addition highway agencies will save even more by the increased life of their pavements and reduced maintenance costs.

From the technology stand point, computer vision is a great tool that can be used to assist roller operators and improve the compaction quality. However like any other technology it has limitations. The biggest shortcoming of this solution is the cumulative error in distance measurement. To avoid this issue the operator has to reset the measurements, once a new rolling zone is started.

Using infra-red camera in this research was a novel approach to overcome some of the limitations of optical vision. This expanded the application of the solution to both day a night jobs.

6.2. RECOMMENDATIONS FOR FURTHER RESEARCH

Vibration is an essential characteristic of rollers used for asphalt compaction. Such vibration induce false motion in the vision and thus adversely affect the results. The vibration was not directly addressed in this research and many of the videos used in this study were recorded while the roller was operated in static mode. For future research, it is recommended considering use of vibration dampeners for the camera setup, as well as investigation of noise reduction with post processing of video streams.

The main part of this research was involved in investigation of the available technologies to replace GPS tracking and software development. Although some field testing was done to evaluate the system performance after development but further testing and evaluation on different types of jobs and comparing the results with GPS based roller pass mapping system can help recognizing the system shortcomings and improving of the performance. Having enough field data tied to the local coordinates, the sensitivity of system performance to the user input parameters must be evaluated.

The IR camera calibration could be further developed. As mentioned in chapter 4, the ellipse correction method by Ellmauthaler et al. [55], is partially incorporated into the software and requires further development for full functionality.

For improved accuracy, the system could be integrated with dead reckoning sensors such as IMUs.

References

[1] Asphalt Institute, The Asphalt Handbook, MS-4, 7th ed., 2007.

[2] J. Cabrera, "Assessment of the Workability of Bituminous Mixtures," *Highways and Transportation*, pp. 17-23, November 1991.

[3] N. McLeod, "Influence of Viscosity of Asphalt Cements on Compaction of Paving Mixtures in the Field," *Highway Research Record No. 158, Highway Research Board*, pp. 76-115, 1967.

[4] B. A. Chadboum, D. E. Newcomb, V. R. Voller, R. A. DeSombre, J. A. Luoma and D. H. Timm, "An Asphalt Paving Tool For Adverse Conditions," Minneapolis, MN, 1998.

[5] J. Luoma, B. Allen, V. Voller and D. Newcomb, "Modeling of Heat Transfer During Asphalt Paving," in *Proceedings, 9th International Conference on Numerical Methods in Thermal Problems*, 1995.

[6] "Warm Mix Asphalt FAQs," FHWA, 12 Aug 2013. [Online]. Available: http://www.fhwa.dot.gov/everydaycounts/technology/asphalt/faqs.cfm. [Accessed 6 Feb 2014].

[7] American Association of State Highway and Transportation Officials;United States;National Research Council (U.S.); Army Corps of Engineering, Hot-Mix Asphalt Paving, Handbook 2000, 2000.

[8] W. Kari, "Mix Properties as They Affect Compaction," *Asphalt Paving Technology Proceedings: Association of Asphalt Paving Technologists Technical Sessions,* vol. 36, pp. 295-309, 1967.

[9] BOMAG, "AsphaltManager," 03 2009. [Online]. Available: www.bomag.com/asphaltmanager/worldwide/downloads/PRE109017_0903.pdf. [Accessed 18 11 2013].

[10] HAMM AG, [Online]. Available: http://media.wirtgen-group.com/media/04_hamm/products/documents/tech_flyer_oscillation_en.pdf. [Accessed January 2016].

[11] "The Geodynamik Compaction Documentation System," *GEODYN,* Sweden, 1985.

[12] G. Chang, Q. Xu, J. Rutledge, B. Horan, L. Michael, D. White and P. Vennapusa, "Accelerated Implementation of Intelligent Compaction Technology for Embankment Subgrade Soils, Aggregate Base, And Asphalt Pavement Materials," Washington, DC, July 2011.

[13] R. Anderegg and K. Kaufmann, "Intelligent Compaction with Vibratory Rollers: Feedback Control Systems in Automatic Compaction and Compaction Control," *Transportation Research Record: Journal of the Transportation Research Board,* vol. 1868, no. 1, pp. 124-134, Jan 2004.

[14] J. A. Scherocman, S. Rakowski and K. Uchiyama, "Intelligent Compaction, Does It Exist?," in *Canadian Technical Asphalt Association (CTAA) Conference*, Victoria, BC, 2007.

[15] A. El-Rabbany, Introduction to GPS: The Global Positioning System, Second Edition ed., Artech House, 2006.

[16] "Using Public-Private Partnerships to Carry Out Highway Projects," January 2012.

[17] "Glossary of Highway Quality Assurance Terms, FOURTH UPDATE," Washington, DC, May 2009.

[18] R. D. Horan, G. K. Chang, Q. Xu and V. L. Gallivan, "Improving Quality Control of Hot-Mix Asphalt Paving with Intelligent Compaction Technology," *Transportation Research Record: Journal of the Transportation Research Board*, vol. 2268, no. 1, pp. 82-91, 2012.

[19] S. Sebesta, T. Scullion and T. Saarenketo, "Using Infrared and High-Speed Ground-Penetrating Radar for Uniformity Measurements on New HMA Layers," Washington, D.C., 2013.

[20] A. Kelly, Mobile Robotics, Mathematics, Models and Methods, New York: Cambridge, 2013.

[21] J.-A. Fernández-Madrigal, Simultaneous Localization and Mapping for Mobile Robots: Introduction and Methods, 1st ed., J. L. Blanco Claraco, Ed., IGI Global, 2012.

[22] E. Rezazadeh Azar, "Computer Vision-based Solution to Monitor Earth Material Loading Activities," Toronto, Ontario , 2013.

[23] J. Borenstein, H. Everett and L. Feng, "Where am I? Sensors and Methods for Mobile Robot Positioning," 1996.

[24] B. Barshan and H. F. Durrant-Whyte, "Inertial Navigation Systems for Mobile Robots," *IEEE TRANSACTIONS ON ROBOTICS AND AUTOMATION,* vol. 11, no. 3, pp. 328-342, June 1995.

[25] T. Cheng, M. Venugopal, J. Teizer and P. Vela, "Performance evaluation of ultra wideband technology for construction resource location tracking in harsh environments," *Automation in Construction,* vol. 20, no. 8, pp. 1173-1184, Dec 2011.

[26] A. Montaser and O. Moselhi, "RFID+ for Tracking Earthmoving Operations," in *Construction Research Congress*, West Lafayette, IN, 2012.

[27] I. Brilakis and L. Soibelman, "Content-Based Search Engines for construction image databases," *Automation in Construction,* vol. 14, no. 4, pp. 537-550, Aug 2005.

[28] V. H. a. R. B. Milan Sonka, Image Processing, Analysis, and Machine Vision. Thomson, 3rd ed., Cengage Learning, 2007.

[29] Z. Hou, K. Wang and W. Gong, "Experimentation of 3D Pavement Imaging through Stereovision," in *International Conference on Transportation Engineering*, 2007.

[30] J. J. Lee, Y. Fukuda, M. Shinozuka, S. Cho and C. Yun, "Development and application of a vision-based displacement measurement system for structural health monitoring of civil structures," *Smart Structures and Systems,* vol. 3, no. 3, pp. 373-384, 2007.

[31] T. Schmidt, J. Tyson and K. Galanulis, "Full-Field Dynamic Displacement and Strain Measurement Using Advanced 3D Image Correlation Photogrammetry," *Experimental Techniques*, vol. 27, no. 3, pp. 47-50, Mar 2006.

[32] S. K. Sinha and P. W. Fieguth, "Computer Vision Techniques for Automatic Structural Assessment of Underground Pipes," *Computer-Aided Civil and Infrastructure Engineering,* vol. 18, no. 2, pp. 95-112, Feb 2003.

[33] A. Papanicolaou, P. Diplas, M. Balakrishnan and C. Dancey, "Computer Vision Technique for Tracking Bed Load Movement," *Journal of Computing in Civil Engineering,* vol. 13, no. 2, p. 71–79, April 1999.

[34] N. Winters, J. Gaspar, G. Lacey and J. Santos-Victor, "Omni-directional vision for robot navigation," in *IEEE Workshop on Omnidirectional Vision*, 2000.

[35] D. Murray and C. Jennings, "Stereo vision based mapping and navigation for mobile robots," in *IEEE International Conference on Robotics and Automation*, 1997.

[36] Q. V. Do, P. Lozo and C. Lakhmi, "Vision-Based Autonomous Robot Navigation," in *Innovations in Robot Mobility and Control, Studies in Computational Intelligence, Volume 8*, S. Patnaik, C. Lakhmi, S. Tzafestas, G. Resconi and A. Konar, Eds., Springer, 2005.

[37] B. Jähne, Digital Image Processing, 6th revised and extended edition ed., Springer, 2005.

[38] M. Sonka, V. Hlavac and R. Boyle, Imaga Processing, Analysis and Machine Vision, 3rd ed., 2008.

[39] J. Canny, "A Computational Approach to Edge Detection," *IEEE Transactions on Pattern Analysis and Machine Intelligence, Vol. Pami-8,,* Vols. PAMI-8, no. 6, November 1986.

[40] C. Harris and M. Stephens, "A Combined Corner and Edge Detector," in *Fourth Alvey Vision Conference,* 1988.

[41] B. Lucas and T. Kanade, "An Iterative Image Registration Technique with an Application to Stereo Vision," in *7th International Conference on Artificial Intelligence (IJCAI),* Vancouver, BC, Aug 1981.

[42] H. Durrant-Whyte and T. Bailey, "Simultaneous localization and mapping: part I," *Robotics & Automation Magazine, IEEE,* vol. 13, no. 2, pp. 99-110, June 2006.

[43] S.-h. Cho and Sangjin Hong, "Map based indoor robot navigation and localization using laser range finder," in *2010 11th International Conference on Control Automation Robotics & Vision (ICARCV),* 7-10 Dec. 2010.

[44] S. Diamantas and R. Crowder, "Localisation and Mapping Using a Laser Range Finder: A Goal-Seeking Approach," in *Fifth International Conference on Autonomic and Autonomous Systems, 2009. ICAS '09,* 20-25 April 2009.

[45] A. Davison, I. Reid, N. Molton and O. Stasse, "MonoSLAM: Real-Time Single Camera SLAM," *IEEE Transactions on Pattern Analysis and Machine Intelligence,* vol. 29, no. 6, pp. 1052-1067, June 2007.

[46] P. McLauchlan and D. Murray, "A unifying framework for structure and motion recovery from image sequences," in *Fifth International Conference on Computer Vision*, 1995.

[47] A. Hernandez-Gutierrez, J. I. Nieto, T. Vidal-Calleja and E. Nebot, "Large scale visual odometry using stereo vision," in *Australasian Conference on Robotics and Automation (ACRA),* Sydney, Australia, December 2009.

[48] A. Davison, "Real-time simultaneous localisation and mapping with a single camera," in *Ninth IEEE International Conference on Computer Vision*, 2003.

[49] M. B. Kitt, J. Rehder, A. D. Chambers, M. Schonbein, H. Lategahn and S. Singh, in *Proc. European Conference on Mobile Robots*, 2011.

[50] S. Lovegrove, A. Davison and J. Ibanez-Guzman, "Accurate Visual Odometry from a Rear Parking Camera," in *IEEE INTELLIGENT VEHICLES SYMPOSIUM*, Baden, Germany, 2011.

[51] Z. Zhang, "A flexible new technique for camera calibration," in *IEEE Transactions on Pattern Analysis and Machine Intelligence*, 2000.

[52] S. Brahmbhatt, Practical OpenCV, Apress; 1st edition, 2013.

[53] R. Hartley and A. Zisserman, Multiple View Geometry in Computer Vision, Cambridge University Press, 2004.

[54] G. Bradski and A. Kaehler, Learning OpenCV, Computer Vision with the OpenCV Library, O'Reilly Media, 2008.

[55] A. Ellmauthaler, E. da Silva, C. Pagliari, J. Gois and S. Neves, "A novel iterative calibration approach for thermal infrared cameras," in *2013 20th IEEE International Conference on Image Processing (ICIP)*, 2013.

[56] M. Gschwandtner and R. Kwitt, "Infrared camera calibration for dense depth map construction," *Intelligent Vehicles Symposium,* vol. (IV), pp. 857-862, 2011 .

[57] J. Campbell, R. Sukthankar, I. Nourbakhsh and A. Pahwa, "A Robust Visual Odometry and Precipice Detection System Using Consumer-grade Monocular Vision," in *IEEE International Conference on Robotics and Automation*, 2005.

[58] BOMAG GmbH, Fayat Group;, Basic Principles of Asphalt Compaction, BOMAG GmbH, Hellerwald, D-56154 Boppard.

[59] "About," OpenCV Developers Team: ITSEEZ, 2013. [Online]. Available: http://opencv.org/about.html. [Accessed Dec Dec 2013].

[60] M. Stroup-Gardiner and E. Brown, "Segregation in Hot Mix Asphalt," Washington, D.C., 1998.

[61] Basics of non contact temperature measurement, Y9766331-A021021DGO ed., MICRO-EPSILON.

[62] R. I. Hammoud, Ed., Augmented Vision Perception in Infrared, London: Springer-Verlag, 2009.

[63] Y. Cho, T. Bode and Y. Kim, "Advanced Quality Control Methods for Road Paving Construction by Utilizing Sensory Devices," in *Construction Research Congress 2009*.

[64] S. R. Miller, A. G. Doree, H. L. Huerne and B. W. Sluer, "Paving the Way Forward: A Case Study in Innovation and Process Control," in *Fourth Annual Eurasphalt and Eurobitume Congress*, Copenhagen, Denmark, May 21–23, 2008.

[65] W. Kröber, E. Floss and W. Wallrath, "Dynamic soil stiffness as quality criterion for soil compaction," in *Geotechnics for Roads, Rail Tracks and Earth Structures*, Tokyo, 2001.

[66] J. McCall and M. Trivedi, "Video-based lane estimation and tracking for driver assistance: survey, system, and evaluation," *IEEE Transactions on Intelligent Transportation Systems,* vol. 7, no. 1, pp. 20-37, March 2006.

[67] S. Woo, D. Hong, W.-C. Lee, J.-H. Chung and T.-H. Kim, "A robotic system for road lane painting," *Automation in Construction,* vol. 17, no. 2, pp. 122-129, January 2008.

[68] S. Sivaraman and M. Trivedi, "Improved vision-based lane tracker performance using vehicle localization," in *Intelligent Vehicles Symposium (IV), 2010 IEEE*, 2010.

[69] M. Grewal and A. Andrews, Kalman Filtering; Theory and Practice, Prentice Hall, 1993.

[70] V. Gallivan, G. Chang and D. Horan, "Intelligent Compaction for Improving Roadway Construction," in *Emerging Technologies for Material, Design, Rehabilitation, and Inspection of Roadway Pavements*.

[71] F. Beainy, S. Commuri and M. Zaman, "Quality Assurance of Hot Mix Asphalt Pavements Using the Intelligent Asphalt Compaction Analyzer," *Journal of Construction Engineering and Management,* vol. 138, no. 2, pp. 178-187, Feb 2012.

[72] S. Commuri and M. Zaman, "A novel neural network-based asphalt compaction analyzer," *International Journal of Pavement Engineering,* vol. 9, no. 3, p. 177–188, 2008.

[73] S.-K. Kim and J. S. Russell, "Framework for an intelligent earthwork system: Part I. System architecture," *Automation in Construction,* vol. 12, no. 1, pp. 1-13, Jan 2003.

[74] Adelo, "http://www.adelo.se/products/," 5 Feb 2014. [Online].

[75] F. L. Roberts, P. S. Kandhal, E. R. Brown, D. Y. Lee and T. W. Kennedy, Hot Mix Asphalt Materials, Mixture Design and Construction, Third ed., Lanham, MD: NAPA Research and Education Foundation, 2009.

[76] FHWA, "Warm Mix Asphalt Technologies and Research," 8 June 2012. [Online]. Available: http://www.fhwa.dot.gov/pavement/asphalt/wma.cfm. [Accessed 10 Feb 2014].

[77] ASTEC, "Products, Drying & Mixing, Double Barrel, Overview," [Online]. Available: http://www.astecinc.com/index.php?option=com_content&view=article&id=109&Itemid=180. [Accessed 10 Feb 2014].

[78] A. Papagiannakis and E. Masad, Pavement Design and Materials, Hoboken: John Wiley, 2008.

[79] A. Sandström and C. Pettersson, "Intelligent systems for QA/QC in soil compaction," in *83rd Annual Transportation Research Board Meeting*, Washington, D.C., January 2004.

[80] D. Adam and F. Kopf, "Operational devices for compaction optimization and quality control (Continuous Compaction Control & Light Falling Weight Device)," in *Intl. Seminar on Geotechnics in Pavement and Railway Design and Construction*, Athens, Greece, December 2004.

[81] "ASTM D8- 13b Standard Terminology Relating to Materials for Roads and Pavements," American Society for Testing and Material, 2013.

[82] K. A. Willoughby, J. P. Mahoney, L. M. Pierce, J. S. Uhlmeyer, K. W. Anderson, S. A. Read, S. T. Muench, T. R. Thompson and R. Moore, "Construction-Related Aaphalt Concrete Pavement Temperature Differentials and the Corresponding Density Differentials," Seattle, Washington, July 2001.

[83] "Test Procedure for Thermal Profile of Hot Mix Asphalt," Texas Department of Transportation, Tex-244-F, 2011.

[84] R. Roberts, C. Potthast and F. Dellaert, "Learning general optical flow subspaces for egomotion estimation and detection of motion anomalies," *IEEE Conference on Computer Vision and Pattern Recognition,* no. CVPR 2009, pp. 57-64, 2009.